Direct Kinematic Singularities and Stability Analysis of Sagging Cable-driven Parallel Robots

Sébastien Briot[1] and Jean-Pierre Merlet[2]

***Abstract*—Sagging cable-driven parallel robots (CDPRs) are often modelled by using the Irvine's model. We will show that their configurations may be unstable, and moreover, that assessing the stability of the robot with the Irvine's model cannot be done by checking the spectrum of a stiffness matrix associated with the platform motions.**

In the present paper, we show that the static configurations of the sagging CDPRs are local extrema of the functional describing the robot potential energy. For assessing the stability, it is then necessary to check two conditions: The Legendre-Clebsch and the Jacobi conditions, both well known in optimal control theory. We will also (i) prove that there is a link between some singularities of the CDPRs and the limits of stability and (ii) show that singularities of the platform wrench system are not singularities of the geometric model of the sagging CDPRs, contrary to what happens in rigid-link parallel robotics.

The stability prediction results are validated in simulation by cross-validating them by using a lumped model, for which the stability can be assessed by analyzing the spectrum of a reduced Hessian matrix of the potential energy.

***Index Terms*—Cable-driven parallel robots, Sagging cables, Stability, Singularity, Optimal control**

I. Introduction

Cable-driven parallel robots (CDPR) are parallel robots whose legs are constituted by cables with lengths that can be changed by an actuation system. CDPRs have been proposed in the seminal papers of Landberger [1] and Albus [2] and have been investigated either because of their large workspace and lifting capacity or because of their possible very high speed [3]. Numerous CDPR prototypes have been developed [4]–[8].

CDPR analysis heavily relies on a cable model, i.e. the relationships between cable tension and shape that are dependent upon the physical characteristics of the cable material. Many works rely on the *straight cable* model in which the cable shape is the line between the two attachment points, the cable has no mass and no elasticity. This model is clearly not realistic for large CDPRs. Moreover with this model, whatever the CDPR size is, the geometry may impose to have a slack cable which does not play a role thereby leading to manage different sets of kinematic equations. Hence, more realistic models, able to tackle with the cable deformations or slackness, are slowly appearing in the literature [9]–[14] and currently the model that is the most used for CDPRs is the one proposed in the Irvine textbook [15], a planar model that relates the cable shape, the tension applied at its extremity and its length at rest (the model will be fully described in a later section) using the Young modulus E and linear density ρ of the cable material. This model has been experimentally shown to be realistic for CDPRs [16] and cables following Irvine's model are named *sagging* cables.

Regarding geometry and kinematics and without going into the details, introducing Irvine's model for a n cable spatial (planar, resp.) CDPR leads to a system of $3n$+6 ($2n$+3, resp.) equations with $3n$ ($2n$, resp.) unknowns for the *inverse kinematics (IK)* (i.e. finding the cable lengths for a given pose of the platform) and hence a square system is obtained only if $n = 6$ ($n = 3$, resp.). Regarding the *direct kinematics (DK)* (i.e. finding the platform pose for given cable lengths), we have the same number of equations and variables, therefore fixing the cable lengths allows to find the platform pose. Solving the *IK* and *DK* for CDPR with sagging cables is not a trivial task and may be based on *continuation* [17], [18] or *interval analysis* [19] although none of these approaches may guarantee to find **all** solutions (at least in a reasonable computation time). Note that in the following of the paper, we will not use the terminology IK/DK which is improper due to the fact that the model equations use both geometric constraints and static equilibrium equations. Therefore we will rather use the terms inverse/direct geometrico-static models which better describe the physics behind the equations.

Sagging CDPRs are by essence underactuated mechanisms, due to the deformable nature of their cables. The geometrico-static equations of these robots involve the mechanical equilibrium of the system and, like any underactuated mechanical systems, computed solutions of the static equilibrium may be stable or unstable (e.g. consider the free-oscillating pendulum). A mechanical equilibrium is well-known to be stable if and only if it corresponds to a minimum of the potential energy of the mechanical system. Otherwise, the computed equilibrium is said to be unstable and it corresponds either to a maximum or a saddle point of the potential energy function. As a result, any small perturbation will move the system towards a more stable configuration.

The stability for CDPR has been analyzed for CDPRs with straight-cables (SC). For instance, in [20], the stability of the underconstrained SC-CDPRs is assessed by checking the positiveness of the reduced Hessian matrix of the potential energy. An approach based on the study of the cable tension and stiffness is proposed in [21] for any SC-CDPRs. In the

*This work was partially supported by the French government, through the French ANR project COSSEROOTS (ANR-20-CE33-0001), the 3IA project Côte d'Azur (ANR-19-P3IA-0002), the ANR project CRAFT (ANR-18-CE10-0004) and the CominLabs project MAMBO.

[1] S. Briot is with the Laboratoire des Sciences du Numérique (LS2N) at the Centre National de la Recherche Scientifique (CNRS), 44321, Nantes, France. Sebastien.Briot@ls2n.fr

[2] J.-P. Merlet is with the Centre de Recherche Inria Sophia Antipolis, 06902 Sophia Antipolis, France. Jean-Pierre.Merlet@inria.fr

work [22], the authors checked the stiffness matrix spectrum of sagging CDPRs for assessing stability, modelled with the Irvine's equations. This stiffness matrix relates the variation of wrenches on the platform (only) to its variation of pose, but any other wrench variations anywhere on the cables, that would destabilize the system, cannot be taken into account. Furthermore, the Irvine's model is the solution of a system of Ordinary Differential Equations (ODEs). Indeed, it is little, if at all, known in the Robotics community that this solution is an *extremum* of a functional (a function of functions) characterizing the total potential energy of the system. Hence, the indices proposed in [22] are not appropriate for assessing the stability of the extrema of a functional. To the best of our knowledge, the stability of sagging CDPRs has not yet been properly investigated.

Indeed, as it was shown in [23] in the case of continuum parallel robots (i.e. parallel robots for which the rigid bodies are replaced by flexible rods which can be modelled thanks to ODEs named the Cosserat equations), proving that the robot configuration is stable can only be done by studying two types conditions which can be found by solving an optimal control problem [24]: the Legendre-Clebsch conditions coupled with the Jacobi conditions.

In this paper, based on the optimal control framework, we provide the mathematical proof that the geometrico-static equations of the sagging CDPRs based in the Irvine's model are the extrema of a functional representing the robot potential energy. Indeed the relation between potential energy and stability appears to be intuitive and has been shown for CDPR with straight cables [20]. However, to the best of our knowledge, there is no proof of it in the literature in the case of the sagging CDPRs. Then, we provide the conditions that are necessary for checking the robot configuration stability, namely the Legendre-Clebsch conditions coupled with the Jacobi conditions. We explain how they may be derived for the sagging CDPR equations. We also prove that there is a link between some singularities of the CDPRs [25] and the limits of the stable configuration domain. Finally, we will show on simulation that singularities of the platform wrench system are not singularities of the geometrico-static models of the sagging CDPRs, contrary to what happens in rigid-link parallel robotics.

The paper is written as follows. In the next section, basics but necessary recalls on optimal control theory are made. In Section III, we show that the Irvine's model is an extremum of the cable potential energy. In Section IV, based on a similar optimal control framework, we derive the equations of the spatial sagging CDPRs and we provide the conditions for stability. In Section V, we show that there is a link between the singularities of the direct kinemato-static model[1] and the Jacobi stability conditions. All the results are confirmed through simulations in Section VI. In the last section, conclusions are drawn.

[1]Following [26], we prefer to replace the word kinetostatic by the word kinemato-static: Indeed, the former is an assembly of the words kinetics and statics, and is not related with our present interest in kinematics, i.e. with the study of the motion.

II. Recalls on calculus of variations and optimal control theory

Let us make here some necessary recalls on the calculus of variations and the optimal control frameworks that will be used in this paper in order to both compute the equations of the geometric model of the sagging CDPRs and to assess the stability of the computed robot configurations.

A. General problem statement

As we will show in the following of this paper, solving the geometric model of a sagging CDPR is equivalent to solving a so-called *fixed-time Bolza problem* in optimal control [24]. Such type of problem takes the generic form:

$$\begin{aligned} \min_{\mathbf{u}(t)} \quad & U = \phi(\mathbf{x}_f) + \int_{t_0}^{t_f} L(\mathbf{x},\mathbf{u},t)dt \\ \text{subject to} \quad & \dot{\mathbf{x}} = \boldsymbol{f}(\mathbf{x},\mathbf{u},t) \\ & \mathbf{x}(t_0) = \mathbf{x}_0 \\ & \boldsymbol{\beta}(\mathbf{x}_f) = \mathbf{0} \end{aligned} \tag{1}$$

where U is a functional, $\mathbf{x} \in \mathbb{R}^n$ is the state vector, $\dot{\mathbf{x}}$ is its derivative with respect to the "time-variable" t, $\mathbf{u} \in \mathbb{R}^m$ is the vector of the "control" inputs, $\boldsymbol{\beta} : \mathbb{R}^n \to \mathbb{R}^p$ is the vector of the general terminal constraints, $\phi(\mathbf{x}_f) : \mathbb{R}^n \to \mathbb{R}$ is the terminal cost, $L : \mathbb{R}^n \times \mathbb{R}^m \times \mathbb{R} \to \mathbb{R}$ is the Lagrangian function[2], $\boldsymbol{f} : \mathbb{R}^n \times \mathbb{R}^m \times \mathbb{R} \to \mathbb{R}^n$ is the state derivative which depends on the state $\mathbf{x}$ itself, but also of the control $\mathbf{u}$ and the time t, $\mathbf{x}_f$ is the final state. Note that a subscript 0 denotes the initial value of a variable throughout the article, while a subscript f is for its final value.

B. First-order necessary conditions

Computing the solutions to the problem (1) is equivalent to finding its *first-order necessary conditions of optimality*. For this, let us form an augmented cost function U' defined by:

$$U' = \phi(\mathbf{x}_f) + \boldsymbol{\nu}^T\boldsymbol{\beta}(\mathbf{x}_f) + \int_{t_0}^{t_f} \Big(L + \boldsymbol{\lambda}^T(\dot{\mathbf{x}} - \boldsymbol{f})\Big)\, dt \tag{2}$$

where $\boldsymbol{\lambda}(t) \in \mathbb{R}^n$ and $\boldsymbol{\nu} \in \mathbb{R}^p$ are two Lagrange multiplier vectors that enforce the differential and terminal constraints. It should be mentioned that $\boldsymbol{\lambda}$ is also called the co-state vector. In this expression and the following ones, some of the function notations have been omitted for reasons of convenience. Expression (2) can be rewritten as:

$$U' = G + \int_{t_0}^{t_f} \Big(H + \boldsymbol{\lambda}^T\dot{\mathbf{x}}\Big)\, dt \tag{3}$$

where H is an Hamiltonian function[3] defined by:

$$H(\mathbf{x},\mathbf{u},\boldsymbol{\lambda},t) = L(\mathbf{x},\mathbf{u},t) - \boldsymbol{\lambda}^T\boldsymbol{f}(\mathbf{x},\mathbf{u},t) \tag{4}$$

[2]We use here the terminology of the control community: This Lagrangian is not necessary the Lagrangian function computed as the difference between the kinetic and potential energies, but a more generic function defining a *cost density*.

[3]Here also, we use here the terminology of the control community: This Hamiltonian is not the mechanical Hamiltonian function.

and G is an augmented terminal cost function which takes the form:

$$G(\mathbf{x}_f, \boldsymbol{\nu}) = \phi(\mathbf{x}_f) + \boldsymbol{\nu}^T \boldsymbol{\beta}(\mathbf{x}_f) \tag{5}$$

From the calculus of variations, we know that a minimum of the functional (2) appears when its variation is null, i.e. when $\delta U' = 0$. From optimal control theory [24], the necessary conditions for local optimality leading to the vanishing of $\delta U'$ are given by:

$$\begin{aligned} \dot{\mathbf{x}} &= \boldsymbol{f}(\mathbf{x}, \mathbf{u}, t) \\ \dot{\boldsymbol{\lambda}} &= H_{\mathbf{x}}^T \\ H_{\mathbf{u}} &= \mathbf{0} \\ \mathbf{x}(t_0) = \mathbf{x}_0,\ \boldsymbol{\lambda}(t_0) &= \boldsymbol{\lambda}_0 \\ \mathbf{b}(\mathbf{x}_f, \boldsymbol{\lambda}_f) = \begin{bmatrix} \boldsymbol{\beta}(\mathbf{x}_f) \\ \boldsymbol{\lambda}_f + G_{\mathbf{x}_f}^T \end{bmatrix} &= \mathbf{0} \end{aligned} \tag{6}$$

where the notation $F_{\mathbf{q}}$ denotes the partial differentiation of any function F with respect to a variable $\mathbf{q}$, i.e. $F_{\mathbf{q}} = \partial F / \partial \mathbf{q}$. Moreover, $\mathbf{b} : \mathbb{R}^n \times \mathbb{R}^n \to \mathbb{R}^n$. These equations are known to be the conventional *first-order necessary conditions for optimality* [24]. This system of equations is square, i.e. there is always the same number of equation as the number of variables/functions $\mathbf{x}(t)$, $\boldsymbol{\lambda}(t)$ and $\boldsymbol{\nu}$ to be found.

Under the hypothesis that $H_{\mathbf{u}} = \mathbf{0}$ can be solved for $\mathbf{u}$, which is always true in the following of the paper, the system of equations (6) becomes a two-point boundary value problem taking the form of a system of Differential Algebraic Equations (DAEs). A solution to these equations is not necessary a local minimizer: in general, it is only an extremum (i.e. it could be a minimum, but also a saddle point or a maximum). For knowing if the solution is a minimizer to the problem (1) (in other word, if the found function is a stable solution), the *second-order optimality conditions* must be checked.

C. Second-order sufficient conditions

In order to establish the fact that the solution to (1) is a local minimum, two conditions must be checked [24]:

- The strong *Legendre-Clebsch condition* which states that $\mathbf{H_{uu}}$ must be always positive definite (strictly), i.e.

$$\mathbf{H_{uu}} \succ 0 \quad \forall t \in [t_0\ t_f] \tag{7}$$

- The *Jacobi condition*, which establishes that the solution is unstable if there is a so-called *conjugate point* at the time t_{cp}, $t_{cp} \in [t_0\ t_f[$ (t_f being necessarily out of the integration interval).

The existence of conjugate points can be determined by analyzing along the interval $[t_0\ t_f[$ certain properties of the matrix $\bar{\mathbf{S}}(t)$ relating the variation $\delta\mathbf{x}(t)$ of the state $\mathbf{x}$ at the time t to the variation $\delta\boldsymbol{\lambda}(t)$ of the Lagrange multipliers $\boldsymbol{\lambda}(t)$ at the same time, such that [24]:

$$\delta\boldsymbol{\lambda}(t) = \bar{\mathbf{S}}(t)\delta\mathbf{x}(t) \tag{8}$$

There is a conjugate point at $t = t_{cp}$, $t_{cp} \in [t_0\ t_f[$, if and only if the inverse of the matrix $\bar{\mathbf{S}}(t)$ is rank deficient at $t = t_{cp}$. The way to compute the matrix $\bar{\mathbf{S}}(t)$ will be detailed in the following of the paper. The reader could also refer to [24] which presents several techniques for its computation.

In what follows, we will apply this theoretical framework to the stability analysis of the sagging CDPRs.

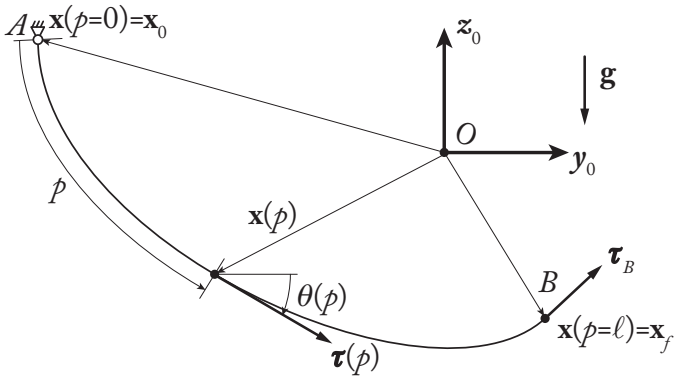

Fig. 1. A sagging cable fixed at one extremity A, subject to an external force at the other extremity B and to the gravity field. $\theta(p)$ is the tangent to the cable at the abscissa p, $\boldsymbol{\tau}(p)$ is the tension in the cable at p, and $\boldsymbol{\tau}_B$ the tenson at B.

III. Deformation equations of a single sagging cable

In this section, we show that the Irvine's model [15] can be found by applying the theory defined in the previous section.

A. Formalization of the problem

Let us consider a single sagging cable in a plane $(O, \boldsymbol{y}_0, \boldsymbol{z}_0)$ (Fig. 1). The cable state vector can be defined as:

$$\mathbf{x}(p) = \begin{bmatrix} y(p) & z(p) \end{bmatrix}^T \in \mathbb{R}^2 \tag{9}$$

where $p \in [0\ \ell]$, p is the curvilinear abscissa along the cable, ℓ is the cable length before deformation, $y(p)$ is the location of a point of the cable at the abscissa p along the $\boldsymbol{y}_0$ axis, and $z(p)$ is the location of a point of the cable at the abscissa p along the $\boldsymbol{z}_0$ axis. Moreover, $\mathbf{x}(p=0) = [y_0\ z_0]^T$ and $\mathbf{x}(p = \ell) = [y_f\ z_f]^T$. The state vector derivative (with respect to the initial curvilinear abscissa prior to any stretching p) is

$$\frac{\partial \mathbf{x}(p)}{\partial p} = \begin{bmatrix} \partial y(p)/\partial p \\ \partial z(p)/\partial p \end{bmatrix} \tag{10}$$

We assume here for the moment, that the vector $\partial\mathbf{x}(p)/\partial p$ is a function of the state $\mathbf{x}$, a control vector $\mathbf{u}$ that we will define below, and of the curvilinear abcissa p, i.e. $\partial\mathbf{x}(p)/\partial p = \boldsymbol{f}(\mathbf{x}, \mathbf{u}, p)$.

In what follows, let us replace the variable $p \in [0\ \ell]$ by a normalized curvilinear abscissa $s \in [0\,1]$ defined by $s = p/\ell$. As a result, we have:

$$\mathbf{x}_i'(s) = \ell \frac{\partial \mathbf{x}}{\partial p} = \ell\, \boldsymbol{f}(\mathbf{x}, \mathbf{u}, s) \tag{11}$$

where the symbol " $'$ " denotes the partial derivative with respect to the curvilinear abscissa s, i.e. $(.)' = \partial(.)/\partial s$.

Let us assume that the cable is extensible, with a cross-section area A and made with a material having a linear density

ρ and a Young's modulus E (assuming a Hookean deformation law). As a result, its deformation energy U_e is provided by the functional [27]:

$$U_e = \ell \int_0^1 \left(\frac{EA}{2} \left(\epsilon_x(s) - 1 \right)^2 \right) ds \tag{12}$$

where $\epsilon_x(s) = \|\partial \mathbf{x}/\partial p\| = \|\mathbf{x}'\|/\ell$ is the elongation strain. In order to fit with the optimal control framework presented in the Section II, let us assume here that the control vector $\mathbf{u}(s) = [u_1(s)\ u_2(s)]^T$ is equal to $\partial \mathbf{x}(p)/\partial p$ such that $u_1 = \partial y/\partial p = \ell y'$ and $u_2 = \partial z/\partial p = \ell z'$, or also $\mathbf{u} = \ell \mathbf{x}' = \ell \boldsymbol{f}$. As a result:

$$\epsilon_x(s) = \|\mathbf{u}(s)\| = \sqrt{u_1^2(s) + u_2^2(s)} \tag{13}$$

and

$$U_e = \ell \int_0^1 \left(\frac{EA}{2} \left(\|\mathbf{u}(s)\| - 1 \right)^2 \right) ds \tag{14}$$

Let us also consider that the cable is subject to a gravity field $\mathbf{g} = -g\,\mathbf{z}_0$ ($g > 0$), and that a force $\boldsymbol{\tau}_B \in \mathbb{R}^2$ is applied at $p = \ell$, i.e. at the location $\mathbf{x}_f$. We assume here that $\boldsymbol{\tau}_B$ is a conservative (constant) force in the world frame. Note that, as we are in statics, $\boldsymbol{\tau}_B$ can however take any value. The potential energy U_w due to these external effects is given by:

$$U_w = -\boldsymbol{\tau}_B^T \mathbf{x}_f + \ell \int_0^1 g\rho z(s)\ ds \tag{15}$$

As a result, the total potential energy $U = U_e + U_w$ is provided by the functional:

$$U = -\boldsymbol{\tau}_B^T \mathbf{x}_f + \ell \int_0^1 \left(\frac{EA}{2} \left(\|\mathbf{u}(s)\| - 1 \right)^2 + g\rho z(s) \right) ds \tag{16}$$

The *static* configuration of the cable must minimize the potential energy U. As a result, the following optimization problem must be solved:

$$\begin{aligned} \min_{\mathbf{u}(s)} \quad & U \\ \text{subject to} \quad & \mathbf{x}' = \boldsymbol{f}(\mathbf{x}, \mathbf{u}, s) \\ & \mathbf{x}(s_0) = \mathbf{x}_0 \end{aligned} \tag{17}$$

This problem is nothing else than a *fixed-time Bolza problem*.

B. First-order conditions of optimality

Applying straightforwardly the equations (6) to the problem (17), and noticing that

$$H = \ell \left(\frac{EA}{2} (\|\mathbf{u}(s)\| - 1)^2 + g\rho z(s) - \boldsymbol{\lambda}^T \boldsymbol{f} \right) \tag{18}$$

we get:

$$\mathbf{x}'(s) = \ell \boldsymbol{f}(\mathbf{x}, \mathbf{u}, s) \tag{19}$$

$$\boldsymbol{\lambda}' = H_{\mathbf{x}}^T \Leftrightarrow \boldsymbol{\lambda}' = \ell \begin{bmatrix} 0 \\ g\rho \end{bmatrix} \tag{20}$$

$$H_{\mathbf{u}} = \mathbf{0} \Leftrightarrow \boldsymbol{\lambda} = EA \frac{\epsilon_x - 1}{\epsilon_x} \mathbf{u} \tag{21}$$

$$\boldsymbol{\lambda}_f = \boldsymbol{\tau}_B \tag{22}$$

From these equations, and making a parallelism with the Irvine's model [15], we see that:

- From (20) and (22), $\boldsymbol{\lambda}$ is nothing else than the tension $\boldsymbol{\tau}$ all along the cable, $\boldsymbol{\lambda} = \boldsymbol{\tau}$.
- From (21), and recalling that $\epsilon_x = \|\mathbf{u}(s)\|$, we can prove that

$$\|\boldsymbol{\lambda}\| = \|\boldsymbol{\tau}\| = EA(\epsilon_x - 1) \tag{23}$$

$$\frac{\lambda_2}{\lambda_1} = \frac{\tau_2}{\tau_1} = \frac{u_2}{u_1} \tag{24}$$

  where λ_i (τ_i, resp.) ($i = 1, 2$) is the ith component of $\boldsymbol{\lambda}$ ($\boldsymbol{\tau}$, resp.). Equation (23) is the Hooke's law used in the Irvine's model while combining Eqs. (23) and (24) we get

$$\mathbf{u} = \epsilon_x \begin{bmatrix} \cos\theta \\ \sin\theta \end{bmatrix} \tag{25}$$

  with $\theta(s) = \tan^{-1}(\tau_2(s)/\tau_1(s))$ being the angle of the vector tangent to the cable defined as it in the Irvine's model (Fig. 1).

So, in order to summarize, the first-order optimality conditions can be written as:

$$\begin{bmatrix} \mathbf{x}'(s) \\ \boldsymbol{\tau}'(s) \end{bmatrix} = \ell \begin{bmatrix} \epsilon_x(s)\cos\theta(s) \\ \epsilon_x(s)\sin\theta(s) \\ 0 \\ g\rho \end{bmatrix} \text{ for } s \in [0\ 1] \tag{26}$$

$$\mathbf{b}(\boldsymbol{\tau}_f) = \boldsymbol{\tau}_f - \boldsymbol{\tau}_B = \mathbf{0} \tag{27}$$

for $\mathbf{x}(0) = \mathbf{x}_0$, $\boldsymbol{\tau}(0) = \boldsymbol{\tau}_0$, with

$$\theta(s) = \tan^{-1}(\tau_2(s)/\tau_1(s)) \tag{28}$$

$$\epsilon_x(s) = \frac{\|\boldsymbol{\tau}(s)\|}{EA} + 1 \tag{29}$$

These equations are nothing else than the well known differential equations defining the Irvine's model [15].

Solving expressions (26) to (29), and assuming that the force vector $\boldsymbol{\tau}_B$ takes the form $\boldsymbol{\tau}_B = [F_y\, F_z]^T$, we can obtain the well known expressions defining the sagging cable configuration $\mathbf{x}(s) = [y(s)\ z(s)]^T$:

$$\begin{aligned} y(s) =& y_0 + \frac{F_y \ell s}{EA} + \frac{|F_y|}{\rho g} \left\{ \sinh^{-1} \left[\frac{F_z - \rho g \ell (1-s)}{F_y} \right] \right. \\ & \left. - \sinh^{-1} \left[\frac{F_z - \rho g \ell}{F_y} \right] \right\} \end{aligned} \tag{30}$$

$$\begin{aligned} z(s) =& z_0 + \frac{F_z \ell s}{EA} + \frac{\rho g \ell^2 s}{EA} \left(\frac{s}{2} - 1 \right) \\ & + \frac{1}{\rho g} \left\{ \sqrt{F_y^2 + \left[F_z - \rho g \ell (1-s) \right]^2} \right. \\ & \left. - \sqrt{F_y^2 + \left[F_z - \rho g \ell \right]^2} \right\} \end{aligned} \tag{31}$$

as well as the expressions of the tension $\boldsymbol{\tau}(s) = [\tau_1(s)\ \tau_2(s)]^T$ all along the cable:

$$\tau_1(s) = F_y \tag{32}$$

$$\tau_2(s) = F_z - \rho g \ell (1-s) \tag{33}$$

As a result, **the optimal control framework allows proving that the Irvine's model is nothing more than an extremum of the cable potential energy**.

After having shown this result, let us deal with the modelling and stability analysis of sagging CDPRs.

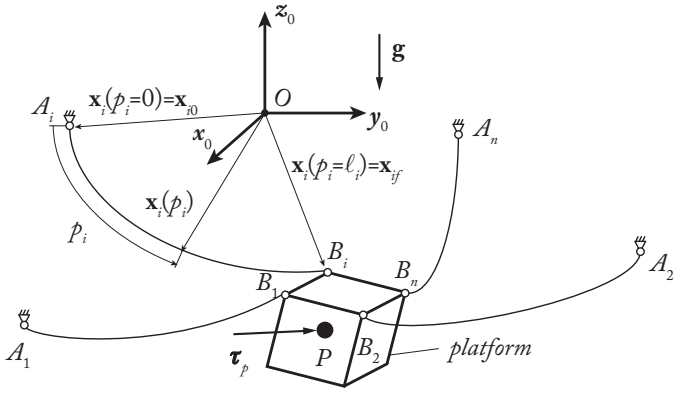

Fig. 2. Schematic representation of a sagging spatial CDPR.

IV. Geometrico-static equations and stability analysis of sagging CDPRs

In this section, we show that the solutions of the geometrico-static model of sagging CDPRs are the extrema of its potential energy, and we derive their stability conditions. We provide the equations for the general spatial case, and discuss how they could be simplified in order to model planar robots.

A. Formalization of the problem

We consider here the general case of a spatial CDPR with sagging cables moving in the space $(O, \boldsymbol{x}_0, \boldsymbol{y}_0, \boldsymbol{z}_0)$ (Fig. 2). The robot is made of n cables connected to a rigid platform. The cable i ($i = 1, \ldots, n$) is connected at point B_i on the platform by a passive spherical joint and at point A_i on the base, a fixed point which is the output point of the winch system[4]. The state vector of the cable i can be defined as:

$$\mathbf{x}_i(p_i) = \begin{bmatrix} x_i(p_i) & y_i(p_i) & z_i(p_i) \end{bmatrix}^T \in \mathbb{R}^3 \tag{34}$$

where p_i is the curvilinear abscissa along the cable, $p_i \in [0\ \ell_i]$, and ℓ_i is the cable length of the undeformed cable. $x_i(p_i)$ ($y_i(p_i)$, $z_i(p_i)$, resp.) is the location of a point of the cable at the abscissa p_i along the $\boldsymbol{x}_0$ ($\boldsymbol{y}_0$, $\boldsymbol{z}_0$, resp) axis. Moreover, the vectors $\mathbf{x}_i(p_i = 0) = \mathbf{x}_{i0}$ and $\mathbf{x}_i(p_i = \ell_i) = \mathbf{x}_{if}$ represent the coordinates of points A_i and B_i in the world frame, respectively. The state vector derivative, with respect to the initial curvilinear abscissa p_i, is given by:

$$\frac{\partial \mathbf{x}_i}{\partial p_i}(p_i) = \begin{bmatrix} \partial x_i(p_i)/\partial p_i \\ \partial y_i(p_i)/\partial p_i \\ \partial z_i(p_i)/\partial p_i \end{bmatrix} \tag{35}$$

We assume again for the moment, that the vector $\partial \mathbf{x}_i(p_i)/\partial p_i$ is a function of the state $\mathbf{x}_i$, a control vector $\mathbf{u}_i$ that we will define below, and of the curvilinear abcissa p_i, i.e. $\partial \mathbf{x}_i(p_i)/\partial p_i = \boldsymbol{f}_i(\mathbf{x}_i, \mathbf{u}_i, p_i)$.

In what follows, it will be necessary to replace again the variable $p_i \in [0\ \ell_i]$ associated with the cable i by a normalized variable $s \in [0\,1]$ defined by $s = p_i/\ell_i$. Therefore we have

$$\mathbf{x}_i'(s) = \ell_i \frac{\partial \mathbf{x}_i}{\partial p_i} = \ell_i\, \boldsymbol{f}_i(\mathbf{x}_i, \mathbf{u}_i, s) \tag{36}$$

[4]For reasons of brevity, we do not consider in the paper any pulley model. We assume that the point A_i is fixed on the base. The following results could be extended to include pulleys.

The platform state is parameterized by the group $\boldsymbol{g}_p = (\mathbf{R}_p, \mathbf{p}_p) \in SE(3)$, where $\mathbf{p}_p$ is vector parameterizing the position of the platform COM P in space and $\mathbf{R}_p$ is the rotation matrix characterizing the rotation of the platform local frame with respect to the world frame. As a result, $\boldsymbol{g}_p$ usually takes the form of an homogeneous transformation matrix characterizing the transformation from the base frame $\mathcal{F}_0$ to the platform frame $\mathcal{F}_p$. In what follows, we use the Lie group parameterization $\boldsymbol{g}_p$ instead of a more classical representation of the platform orientation with angles as it leads to a more natural derivation of the robot mechanical equilibrium equations than any other set of vectorial coordinates, as it will shown further. The location of points B_i in the platform frame are given by the constant vector ${}^p\overrightarrow{PB_i}$, while in the world frame, ${}^0\overrightarrow{PB_i} = \mathbf{R}_p\, {}^p\overrightarrow{PB_i}$[5].

Finally, the geometric loop-closure constraints of the robot can be written under the form $\boldsymbol{\beta} = [\boldsymbol{\beta}_1^T \ldots \boldsymbol{\beta}_n^T]^T = \mathbf{0}$ where

$$\boldsymbol{\beta}_i(\boldsymbol{g}_p, \mathbf{x}_{if}) = \mathbf{p}_p + \mathbf{R}_p\, {}^p\overrightarrow{PB_i} - \mathbf{x}_{if} = \mathbf{0} \tag{37}$$

Again, let us assume that all cables are extensible and, for reasons of brevity, that they have all the same cross-section area A and that they are made with the same material having a linear density ρ and a Young's modulus E (assuming a Hookean deformation law). Moreover, we consider that the CDPR is subject to a gravity field $\mathbf{g} = -g\,\boldsymbol{z}_0$ ($g > 0$). Finally, a pure constant force $\boldsymbol{\tau}_p$ in the world frame is applied at the platform COM ($\boldsymbol{\tau}_p$ includes the gravity force on the platform); We disregard the case of external moments applied on the platform, as moments in the spatial case are non conservative and cannot lead to the definition of a potential energy [28]. Stability analysis with nonconservative loadings requires a different framework and definition of stability in terms of dynamics [29], which is left as a future work. The total potential energy of the CDPR is thus given by the functional:

$$U = \sum_{i=1}^{n} \ell_i \int_0^1 \left(\frac{EA}{2}(\epsilon_{ix} - 1)^2 + g\rho z_i(s) \right) ds - \boldsymbol{\tau}_p^T \mathbf{p}_p \tag{38}$$

where

$$\epsilon_{ix} = \|\mathbf{u}_i(s)\| \,(= \ell_i \|\mathbf{x}_i'(s)\|) \tag{39}$$

is the strain in the cable i.

The *static* (stable) configuration of the spatial CDPR must locally minimize the potential energy U, leading to the following optimization problem:

$$\begin{aligned} \min_{\mathbf{u}(s)} \quad & U \\ \text{subject to} \quad & \mathbf{x}_i{}' = \ell_i \boldsymbol{f}_i(\mathbf{x}_i, \mathbf{u}_i, s) \text{ for } i = 1, \ldots, n \\ & \mathbf{x}_i(s_0) = \mathbf{x}_{i0} \\ & \boldsymbol{\beta}_i(\boldsymbol{g}_p, \mathbf{x}_{if}) = \mathbf{0} \end{aligned} \tag{40}$$

where $\mathbf{u} = [\mathbf{u}_1^T \ldots \mathbf{u}_n^T]^T$. Problems (6) and (40) look similar, but they differ by the fact that the CDPR platform configuration is defined by a group in the spatial case, no more by a vector field. As a result, the computation of the solution

[5]In what follows, a superscript "p" will denote a vector in the platform frame while a superscript "0" will be for the world frame.

slightly differs by its expression. We detail the resolution of the problem (40) below.

B. First-order conditions of optimality

For solving the problem (40), we now define the augmented cost function:

$$U' = G(\boldsymbol{g}_p, \mathbf{x}_{1f}, \dots, \mathbf{x}_{nf}) + \sum_{i=1}^{n} \int_0^1 \left(H_i(\mathbf{x}_i, \mathbf{u}_i, \boldsymbol{\lambda}_i, s) + \boldsymbol{\lambda}_i^T \mathbf{x}_i' \right) ds \quad (41)$$

where

$$G = -\boldsymbol{\tau}_p^T \mathbf{p}_p + \boldsymbol{\beta}^T \boldsymbol{\nu} = -\boldsymbol{\tau}_p^T \mathbf{p}_p + \sum_{i=1}^{n} \boldsymbol{\beta}_i^T \boldsymbol{\nu}_i \quad (42)$$

and $\boldsymbol{\beta} = [\boldsymbol{\beta}_1^T \dots \boldsymbol{\beta}_n^T]^T \in \mathbb{R}^{3n}$. In these equations, $\boldsymbol{\lambda}_i \in \mathbb{R}^3$ and $\boldsymbol{\nu} = [\boldsymbol{\nu}_1^T \dots \boldsymbol{\nu}_n^T]^T \in \mathbb{R}^{3n}$ are two set of Lagrange multipliers. Moreover,

$$H_i = \ell_i \left(\frac{EA}{2} (\|\mathbf{u}_i\| - 1)^2 + g\rho z_i - \boldsymbol{\lambda}_i^T \boldsymbol{f}_i \right) \quad (43)$$

Taking the first variation of U' leads to [30]:

$$\delta U' = \text{tr}\left(G_{\boldsymbol{g}_p}^T \delta \boldsymbol{g}_p \right) + \sum_{i=1}^{n} G_{\mathbf{x}_{if}} \delta \mathbf{x}_{if} + \boldsymbol{\beta}^T \delta \boldsymbol{\nu} + \sum_{i=1}^{n} \int_0^1 (H_{i\mathbf{x}_i} \delta \mathbf{x}_i + H_{i\mathbf{u}_i} \delta \mathbf{u}_i + (H_{i\boldsymbol{\lambda}_i} + \mathbf{x}_i'^T) \delta \boldsymbol{\lambda}_i + \boldsymbol{\lambda}_i^T \delta \mathbf{x}_i' \Big) ds \quad (44)$$

where the term $\text{tr}\left(G_{\boldsymbol{g}_p}^T \delta \boldsymbol{g}_p \right)$, in which tr(.) is the matrix trace operator, corresponds to the variation of the function U' with respect to a variation on the group (see example 3.74 in [30]). The term $\text{tr}\left(G_{\boldsymbol{g}_p}^T \delta \boldsymbol{g}_p \right)$ is also called the *trace pairing* operator, which provides the proper expression for our scalar variation. Moreover, for any matrix $\mathbf{M} \in \mathbb{R}^{a \times b}$ and any scalar function F, the partial derivative $F_{\mathbf{M}}$ is given by:

$$F_{\mathbf{M}} = \frac{\partial F}{\partial \mathbf{M}} = \begin{bmatrix} F_{M_{11}} & \dots & F_{M_{1b}} \\ \vdots & \ddots & \vdots \\ F_{M_{a1}} & \dots & F_{M_{ab}} \end{bmatrix} \quad (45)$$

M_{jk} being the component on the jth row and kth column of $\mathbf{M}$.

Let us now define the variation $\delta \boldsymbol{\Sigma}_p$ as $\delta \boldsymbol{\Sigma}_p = \left(\boldsymbol{g}_p^{-1} \delta \boldsymbol{g}_p \right)^\vee \in se(3) \simeq \mathbb{R}^6$, or also $\delta \boldsymbol{g}_p = \boldsymbol{g}_p \widehat{\delta \boldsymbol{\Sigma}}$, where the symbols $\vee$ and $\wedge$ are Lie group notations that are recalled in the Appendix A for reasons of clarity. $\delta \boldsymbol{\Sigma}_p$ must be seen as *space-twist* characterizing the variation of the platform configuration *in its mobile frame*.

From Section 7.2 in [30], we know that

$$\text{tr}\left(G_{\boldsymbol{g}_p}^T \delta \boldsymbol{g}_p \right) = \mathbf{C}_p \delta \boldsymbol{\Sigma}_p \quad (46)$$

where

$$\mathbf{C}_p = \begin{bmatrix} G_{\mathbf{p}_p}^T \mathbf{R}_\text{p} & \left(\mathbf{R}_\text{p}^T G_{\mathbf{R}_\text{p}} - G_{\mathbf{R}_\text{p}}^T \mathbf{R}_\text{p} \right)^{\vee T} \end{bmatrix} \in \mathbb{R}^{1 \times 6} \quad (47)$$

As a result, by introducing (46) into (44), and by integrating by parts the last term in the integrand, we get:

$$\delta U' = \mathbf{C}_p \delta \boldsymbol{\Sigma}_p + \sum_{i=1}^{n} (G_{\mathbf{x}_{if}} + \boldsymbol{\lambda}_{if}^T) \delta \mathbf{x}_{if} + \boldsymbol{\beta}^T \delta \boldsymbol{\nu} + \sum_{i=1}^{n} \int_0^1 \Big((H_{i\mathbf{x}_i} - \boldsymbol{\lambda}_i'^T) \delta \mathbf{x}_i + H_{i\mathbf{u}_i} \delta \mathbf{u}_i + (H_{i\boldsymbol{\lambda}_i} + \mathbf{x}_i'^T) \delta \boldsymbol{\lambda}_i \Big) ds \quad (48)$$

from which the first-order conditions of optimality can be found [24], for $i = 1, \dots, n$:

$$\mathbf{x}_i' = \ell_i \boldsymbol{f}_i(\mathbf{x}_i, \mathbf{u}_i, s) \quad (49)$$

$$\boldsymbol{\lambda}_i' = H_{i\mathbf{x}_i}^T \quad (50)$$

$$H_{i\mathbf{u}_i} = \mathbf{0} \quad (51)$$

$$\boldsymbol{\lambda}_{if} = -G_{\mathbf{x}_{if}}^T \quad (52)$$

$$\mathbf{C}_p^T = \mathbf{0} \quad (53)$$

$$\boldsymbol{\beta} = \mathbf{0} \quad (54)$$

Here again, it appears that $\boldsymbol{\lambda}_i = \boldsymbol{\tau}_i$ (the tension in cable i) and that $\boldsymbol{\lambda}_{if} = \boldsymbol{\tau}_{B_i}$ the tension in cable i at B_i. Equation (52) leads also to $\boldsymbol{\lambda}_{if} = \boldsymbol{\tau}_{B_i} = \boldsymbol{\nu}_i$, while, after simplifications, Eq. (53) gives

$$\mathbf{0} = -\begin{bmatrix} \boldsymbol{\tau}_p \\ \mathbf{0} \end{bmatrix} + \sum_{i=1}^{n} \begin{bmatrix} \mathbf{I}_3 \\ [^0\overrightarrow{PB_i}]^\wedge \end{bmatrix} \boldsymbol{\tau}_{B_i} \quad (55)$$

which describes the static equilibrium on the platform. Moreover, expanding (51), we have

$$\boldsymbol{\tau}_i = EA \frac{\epsilon_{ix} - 1}{\epsilon_{ix}} \mathbf{u}_i \quad (56)$$

leading to

$$\begin{cases} \|\boldsymbol{\tau}_i\| = & EA(\epsilon_{ix} - 1) \\ \tau_{ij}/\tau_{ik} = & \lambda_{ij}/\lambda_{ik} = u_{ij}/u_{ik} \text{ for } j,k = 1,2,3 \end{cases} \quad (57)$$

where $\lambda_{i\alpha}$ ($\tau_{i\alpha}$, resp.) ($\alpha = j, k$) is the αth component of $\boldsymbol{\lambda}_i$ ($\boldsymbol{\tau}_i$, resp.).

The first line of Eq. (57) is again the Hooke's law while the second line allows to define two angles θ_i and γ_i such that:

$$\gamma_i(s) = \tan^{-1}\left(\frac{\tau_{i2}(s)}{\tau_{i1}(s)} \right)$$
$$\theta_i(s) = \tan^{-1}\left(\frac{\tau_{i3}(s)}{\tau_{i1}(s)\cos\gamma_i(s) + \tau_{i2}(s)\sin\gamma_i(s)} \right) \quad (58)$$

By combining Eqs. (57) and (58), and we can find that:

$$\mathbf{u}_i(s) = \epsilon_{ix}(s) \begin{bmatrix} \cos\theta_i(s)\cos\gamma_i(s) \\ \cos\theta_i(s)\sin\gamma_i(s) \\ -\sin\theta_i(s) \end{bmatrix} \quad (59)$$

So, in order to summarize, the first-order optimality conditions can be written as:

$$\begin{bmatrix}\mathbf{x}_i'(s)\\ \boldsymbol{\tau}_i'(s)\end{bmatrix} = \ell_i \begin{bmatrix}\epsilon_{ix}(s)\cos\theta_i(s)\cos\gamma_i(s)\\ \epsilon_{ix}(s)\cos\theta_i(s)\sin\gamma_i(s)\\ -\epsilon_{ix}(s)\sin\theta_i(s)\\ 0\\ 0\\ g\rho\end{bmatrix} \text{ for } s\in[0\ 1]$$

$$\text{with } \mathbf{x}_i(0)=\mathbf{x}_{i0},\ \boldsymbol{\tau}_i(0)=\boldsymbol{\tau}_{i0},\ i=1,\dots,n \tag{60}$$

$$\text{and } \mathbf{b}=\begin{bmatrix}\boldsymbol{\beta}\\ -\begin{bmatrix}\boldsymbol{\tau}_p\\ \mathbf{0}\end{bmatrix}+\sum_{i=1}^{n}\begin{bmatrix}\mathbf{I}_3\\ [^0\overrightarrow{PB_i}]^\wedge\end{bmatrix}\boldsymbol{\tau}_{B_i}\end{bmatrix}=\mathbf{0} \tag{61}$$

with $\mathbf{b}=\mathbf{b}(\boldsymbol{g}_p,\mathbf{x}_f,\boldsymbol{\tau}_B)\in\mathbb{R}^{3n+6}$, ϵ_{ix} defined by

$$\epsilon_{ix}(s)=\frac{\|\boldsymbol{\tau}_i(s)\|}{EA}+1 \tag{62}$$

and the angles θ_i and γ_i defined in (58). Here, $\mathbf{b}$ is a vector stacking both the geometric loop-closure constraints on the locations of the points B_i and the platform mechanical equilibrium. It should be noted that the solution to (60) is no more given by (31) but by:

$$x_i(s)=x_{i0}+d_i(s)\cos\gamma_i \tag{63}$$

$$y_i(s)=y_{i0}+d_i(s)\sin\gamma_i \tag{64}$$

$$\begin{aligned}z_i(s)=&z_{i0}+\frac{F_{iz}\ell_i s}{EA}+\frac{\rho g\ell_i^2 s}{EA}\left(\frac{s}{2}-1\right)\\&+\frac{1}{\rho g}\left\{\sqrt{F_{ixy}^2+\left[F_{iz}-\rho g\ell_i(1-s)\right]^2}\right.\\&\left.-\sqrt{F_{ixy}^2+\left[F_{iz}-\rho g\ell_i\right]^2}\right\}\end{aligned} \tag{65}$$

with

$$\gamma_i(s)=\tan^{-1}\left(\frac{F_{iy}}{F_{ix}}\right)=const \tag{66}$$

$$F_{ixy}=F_{ix}\cos\gamma_i+F_{iy}\sin\gamma_i=const \tag{67}$$

$$\begin{aligned}d_i(s)=&\frac{|F_{ixy}|}{\rho g}\left\{\sinh^{-1}\left[\frac{F_{iz}-\rho g\ell_i(1-s)}{F_{ixy}}\right]\right.\\&\left.-\sinh^{-1}\left[\frac{F_{iz}-\rho g\ell_i}{F_{ixy}}\right]\right\}+\frac{F_{ixy}\ell_i s}{EA}\end{aligned} \tag{68}$$

and

$$\tau_{i1}(s)=F_{ix} \tag{69}$$

$$\tau_{i2}(s)=F_{iy} \tag{70}$$

$$\tau_{i3}(s)=F_{iz}-\rho g\ell_i(1-s) \tag{71}$$

where $\boldsymbol{\tau}_{B_i}=[F_{ix}\ F_{iy}\ F_{iz}]^T$ and $\boldsymbol{\tau}_i=[\tau_{i1}\ \tau_{i2}\ \tau_{i3}]^T$. It should be mentioned that, by projecting the equations (63) to (71) in a frame attached to the vertical plane passing through the points A_i and B_i, we will found again the equations (26) to (29) of the planar cable.

Based on the explicit relationships (63) to (71) and the boundary conditions $\mathbf{b}=\mathbf{0}$ in (61), the geometrico-static model can be solved by using a numerical solver. In such a case, the unknown to be found would be either the cable lengths are rest ℓ_i and the cable tensions $\boldsymbol{\tau}_{B_i}$ $(i=1,\dots,n)$ for the inverse geometrico-static model [31], or the platform pose $\boldsymbol{g}_p$ and the tensions $\boldsymbol{\tau}_{B_i}$ for the forward geometrico-static model [32]. Note that these problems may have both multiple solutions, and finding all their solutions is a rather complicated task.

C. Second-order conditions of optimality

Here, we study the stability conditions of the sagging CDPR.

1) Legendre-Clebsch conditions: We need to check the positive-definiteness of the block-diagonal matrix $\mathbf{H_{uu}}$ whose expression is:

$$\mathbf{H_{uu}}=\begin{bmatrix}\mathbf{H}_{\mathbf{u}_1\mathbf{u}_1} & \dots & \mathbf{0}\\ \vdots & \ddots & \vdots\\ \mathbf{0} & \dots & \mathbf{H}_{\mathbf{u}_n\mathbf{u}_n}\end{bmatrix} \tag{72}$$

where

$$\mathbf{H}_{\mathbf{u}_i\mathbf{u}_i}=AE\ell_i\begin{bmatrix}\frac{\epsilon_{ix}^3-u_{i2}^2-u_{i3}^2}{\epsilon_{ix}^3} & \frac{u_{i1}u_{i2}}{\epsilon_{ix}^3} & \frac{u_{i1}u_{i3}}{\epsilon_{ix}^3}\\ \frac{u_{i1}u_{i2}}{\epsilon_{ix}^3} & \frac{\epsilon_{ix}^3-u_{i1}^2-u_{i3}^2}{\epsilon_{ix}^3} & \frac{u_{i2}u_{i3}}{\epsilon_{ix}^3}\\ \frac{u_{i1}u_{i3}}{\epsilon_{ix}^3} & \frac{u_{i2}u_{i3}}{\epsilon_{ix}^3} & \frac{\epsilon_{ix}^3-u_{i1}^2-u_{i2}^2}{\epsilon_{ix}^3}\end{bmatrix} \tag{73}$$

with u_{ij} the jth component of $\mathbf{u}_i$ $(j=1,2,3,\ i=1,\dots,n)$. As a result, the eigenvalues of $\mathbf{H_{uu}}$ are identical to the eigenvalues of all matrices $\mathbf{H}_{\mathbf{u}_i\mathbf{u}_i}$ $(i=1,\dots,n)$. An eigenvalue of $\mathbf{H}_{\mathbf{u}_i\mathbf{u}_i}$ is equal to the constant value $AE\ell_i$ while the two others are both equal to:

$$\sigma_i=AE\ell_i\frac{\epsilon_{ix}-1}{\epsilon_{ix}} \text{ for } i=1,\dots,n \tag{74}$$

From Equation (29), $\epsilon_{ix}>1$, except if the cable tension $\boldsymbol{\tau}(t)$ is null, which is unfeasible in practice on Earth (in statics), as long as we are not in the water. Therefore, we always have $\mathbf{H_{uu}}\succ 0$.

2) Jacobi conditions: In order to compute the Jacobi conditions and to verify the presence or not of conjugate points, it is necessary to compute the relation between the variations $\delta\boldsymbol{\tau}(s)$ and $\delta\mathbf{x}(s)$, as explained in Section II-C. For obtaining it, by taking into account that the vector $\mathbf{b}$ of the geometrical and equilibrium constraints is an explicit function $\boldsymbol{g}_p$, $\mathbf{x}_f$ and $\boldsymbol{\tau}_B$ only, let us express its variation $\delta\mathbf{b}$ as:

$$\delta\mathbf{b}=\mathbf{0}=\begin{bmatrix}\text{tr}\left(b_{1\,\boldsymbol{g}_p}^T\delta\boldsymbol{g}_p\right)\\ \vdots\\ \text{tr}\left(b_{3n+6\,\boldsymbol{g}_p}^T\delta\boldsymbol{g}_p\right)\end{bmatrix}+\mathbf{b}_{\mathbf{x}_f}\delta\mathbf{x}_f+\mathbf{b}_{\boldsymbol{\tau}_B}\delta\boldsymbol{\tau}_B \tag{75}$$

where b_k $(k=1,\dots,3n+6)$ is the kth component of the vector $\mathbf{b}$, and $b_{k\,\boldsymbol{g}_p}$ the derivative of b_k with respect to $\boldsymbol{g}_p$, and $\delta\mathbf{x}_f=[\delta\mathbf{x}_{1f}^T\dots\delta\mathbf{x}_{nf}^T]^T\in\mathbb{R}^{3n}$, $\delta\boldsymbol{\tau}_B=[\delta\boldsymbol{\tau}_{B_1}^T\dots\delta\boldsymbol{\tau}_{B_n}^T]^T\in\mathbb{R}^{3n}$,

$$\mathbf{b}_{\mathbf{x}_f}=\begin{bmatrix}-\mathbf{1}_{3n}\\ \mathbf{0}_{6\times 3n}\end{bmatrix}\in\mathbb{R}^{(3n+6)\times 3n} \tag{76}$$

$$\mathbf{b}_{\boldsymbol{\tau}_B}=\begin{bmatrix}\mathbf{0}_{3n\times 3n}\\ \begin{bmatrix}\mathbf{1}_3 & \dots & \mathbf{1}_3\\ [^0\overrightarrow{PB_1}]^\wedge & \dots & [^0\overrightarrow{PB_n}]^\wedge\end{bmatrix}\end{bmatrix}\in\mathbb{R}^{(3n+6)\times 3n} \tag{77}$$

where $\mathbf{1}_3$ ($\mathbf{1}_{3n}$, resp.) is the identity matrix of dimension 3 ($3n$, resp.) and $\mathbf{0}_{6\times 3n}$ the zero matrix of dimension $(6\times 3n)$.

Then, noticing from [30] that

$$\text{tr}\left(b_{k\,\boldsymbol{g}_p}\delta\boldsymbol{g}_p\right)=\mathbf{C}_k\delta\boldsymbol{\Sigma}_p \tag{78}$$

where

$$\mathbf{C}_k=\begin{bmatrix} b^T_{k\,\mathbf{p}_p}\mathbf{R}_\text{p} & \left(\mathbf{R}^T_\text{p}b_{k\,\mathbf{R}_\text{p}}-b^T_{k\,\mathbf{R}_\text{p}}\mathbf{R}_\text{p}\right)^{\vee T}\end{bmatrix}\in\mathbb{R}^{1\times 6} \tag{79}$$

we finally get:

$$\delta\mathbf{b}=\mathbf{0}=\mathbf{J}_p\delta\boldsymbol{\Sigma}_p+\mathbf{b}_{\mathbf{x}_f}\delta\mathbf{x}_f+\mathbf{b}_{\boldsymbol{\tau}_B}\delta\boldsymbol{\tau}_B \tag{80}$$

where

$$\mathbf{J}_p=\begin{bmatrix}\mathbf{C}_1\\ \vdots\\ \mathbf{C}_{3n+6}\end{bmatrix}\in\mathbb{R}^{(3n+6)\times 6} \tag{81}$$

Simplifying (81), it can be proven that:

$$\mathbf{J}_p=\begin{bmatrix}\mathbf{R}_p & -[^0\overrightarrow{PB_1}]^\wedge\mathbf{R}_p\\ \vdots & \vdots\\ \mathbf{R}_p & -[^0\overrightarrow{PB_n}]^\wedge\mathbf{R}_p\\ \mathbf{0}_{3\times 3} & \mathbf{0}_{3\times 3}\\ \mathbf{0}_{3\times 3} & \sum_{i=1}^n(^0\overrightarrow{PB_i}\boldsymbol{\tau}^T_{B_i}-(^0\overrightarrow{PB_i}^T\boldsymbol{\tau}_{B_i})\mathbf{1}_3)\mathbf{R}_p\end{bmatrix} \tag{82}$$

Relating $\delta\mathbf{x}_f$ and $\delta\boldsymbol{\tau}_B$ to $\delta\mathbf{x}(s)$ and $\delta\boldsymbol{\tau}(s)$: Let us now calculate the so-called "transition matrix" $\boldsymbol{\Phi}(t,t_f)$ of the DAE (60) which relates $\delta\mathbf{x}_f$ and $\delta\boldsymbol{\tau}_B$ to $\delta\mathbf{x}(s)$ and $\delta\boldsymbol{\tau}(s)$ such that [24]:

$$\begin{bmatrix}\delta\mathbf{x}(s)\\ \delta\boldsymbol{\tau}(s)\end{bmatrix}=\boldsymbol{\Phi}(s,s_f=1)\begin{bmatrix}\delta\mathbf{x}_f\\ \delta\boldsymbol{\tau}_B\end{bmatrix} \tag{83}$$

where

$$\boldsymbol{\Phi}(s,s_f=1)=\begin{bmatrix}\frac{\partial\mathbf{x}(s)}{\partial\mathbf{x}_f} & \frac{\partial\mathbf{x}(s)}{\partial\boldsymbol{\tau}_B}\\ \frac{\partial\boldsymbol{\tau}(s)}{\partial\mathbf{x}_f} & \frac{\partial\boldsymbol{\tau}(s)}{\partial\boldsymbol{\tau}_B}\end{bmatrix} \tag{84}$$

In general, the transition matrix $\boldsymbol{\Phi}(s,s_f=1)\in\mathbb{R}^{6n\times 6n}$ can be only obtained using a numerical procedure, that will not be detailed here. The interesting reader could refer to [24] for further information on it. In our study, an analytical form of $\boldsymbol{\Phi}(t,t_f)$ can be obtained as follows.

Analyzing Equations (63) to (71), we see that the vectors $\mathbf{x}(s)$ and $\boldsymbol{\tau}(s)$ are explicit functions of $\mathbf{x}_0$ and $\boldsymbol{\tau}_B$ and that

$$\frac{\partial\mathbf{x}(s)}{\partial\mathbf{x}_0}=\mathbf{1}_{3n},\ \frac{\partial\boldsymbol{\tau}(s)}{\partial\mathbf{x}_0}=\mathbf{0},\ \frac{\partial\boldsymbol{\tau}(s)}{\partial\boldsymbol{\tau}_B}=\mathbf{1}_{3n} \tag{85}$$

Moreover, expressing Equations (63) to (65) at $s=1$, it comes that

$$\frac{\partial\mathbf{x}_f}{\partial\mathbf{x}_0}=\mathbf{1}_{3n}\Rightarrow\frac{\partial\mathbf{x}(s)}{\partial\mathbf{x}_f}=\mathbf{1}_{3n}\text{ and }\frac{\partial\boldsymbol{\tau}(s)}{\partial\mathbf{x}_f}=\mathbf{0} \tag{86}$$

Finally, the last component $\frac{\partial\mathbf{x}(s)}{\partial\boldsymbol{\tau}_B}$ of $\boldsymbol{\Phi}(s,s_f=1)$ can be obtained by a direct differentiation of the equations (63) to (65) with respect to the vector $\boldsymbol{\tau}_B$. Its expression is rather long and will not be displayed for reasons of brevity, but it can be obtained in a straightforward manner following the previous comment.

Introducing (83) into (80), we then get:

$$\delta\mathbf{b}=\mathbf{0}=\mathbf{J}_p\delta\boldsymbol{\Sigma}_p+\mathbf{b}_{\mathbf{x}(s)}\delta\mathbf{x}(s)+\mathbf{b}_{\boldsymbol{\tau}(s)}\delta\boldsymbol{\tau}(s) \tag{87}$$

where

$$\mathbf{b}_{\mathbf{x}(s)}=\mathbf{b}_{\mathbf{x}_f}\left(\boldsymbol{\Phi}^{-1}\right)_{11}+\mathbf{b}_{\boldsymbol{\tau}_B}\left(\boldsymbol{\Phi}^{-1}\right)_{21} \tag{88}$$

and

$$\mathbf{b}_{\boldsymbol{\tau}(s)}=\mathbf{b}_{\mathbf{x}_f}\left(\boldsymbol{\Phi}^{-1}\right)_{12}+\mathbf{b}_{\boldsymbol{\tau}_B}\left(\boldsymbol{\Phi}^{-1}\right)_{22} \tag{89}$$

where the matrices $\left(\boldsymbol{\Phi}^{-1}\right)_{11}\in\mathbb{R}^{3n\times 3n}$ and $\left(\boldsymbol{\Phi}^{-1}\right)_{21}\in\mathbb{R}^{3n\times 3n}$ ($\left(\boldsymbol{\Phi}^{-1}\right)_{12}\in\mathbb{R}^{3n\times 3n}$ and $\left(\boldsymbol{\Phi}^{-1}\right)_{22}\in\mathbb{R}^{3n\times 3n}$, resp.) are the upper left and lower left blocks (the upper right and lower right blocks, resp.) of the matrix $\boldsymbol{\Phi}^{-1}(s,s_f)$, respectively.

Computation of the Jacobi conditions: Finally, let us find the expression of the matrix $\bar{\mathbf{S}}(s)$ for checking the presence of conjugate points. For this, let us first define the matrix $\mathbf{Z}$ which spans the nullspace of the matrix $\mathbf{J}_p^T$, i.e.

$$\mathbf{J}_p^T\mathbf{Z}=\mathbf{0} \tag{90}$$

Assuming that $\mathbf{J}_p$ is of full rank, which is true as long as all points B_i are not all aligned, then $\mathbf{Z}\in\mathbb{R}^{(3n+6)\times 3n}$. Left-multiplying (87) by $\mathbf{Z}^T$, we get

$$\mathbf{0}=\mathbf{Z}^T\mathbf{b}_{\mathbf{x}(s)}\delta\mathbf{x}(s)+\mathbf{Z}^T\mathbf{b}_{\boldsymbol{\tau}(s)}\delta\boldsymbol{\tau}(s) \tag{91}$$

where here $\mathbf{Z}^T\mathbf{b}_{\mathbf{x}(s)}\in\mathbb{R}^{3n\times 3n}$ and $\mathbf{Z}^T\mathbf{b}_{\boldsymbol{\tau}(s)}\in\mathbb{R}^{3n\times 3n}$. Then it comes that:

$$\delta\boldsymbol{\tau}(s)=-\left(\mathbf{Z}^T\mathbf{b}_{\boldsymbol{\tau}(s)}\right)^{-1}\left(\mathbf{Z}^T\mathbf{b}_{\mathbf{x}(s)}\right)\delta\mathbf{x}(s) \tag{92}$$

and, by identification with (8):

$$\bar{\mathbf{S}}(t)=-\left(\mathbf{Z}^T\mathbf{b}_{\boldsymbol{\tau}(s)}\right)^{-1}\left(\mathbf{Z}^T\mathbf{b}_{\mathbf{x}(s)}\right) \tag{93}$$

This expression results in the fact that there is a conjugate point at $s=s_{cp}$ only if the matrix $\mathbf{Z}^T\mathbf{b}_{\boldsymbol{\tau}(s)}$ is singular at $s=s_{cp}$, as long as $\mathbf{Z}^T\mathbf{b}_{\mathbf{x}(s)}$ is finite (which is true under the mild and verifiable assumption that $\frac{\partial\mathbf{b}}{\partial\mathbf{x}_f}$ and $\frac{\partial\mathbf{b}}{\partial\boldsymbol{\tau}_B}$ are finite when evaluated at $\mathbf{x}_f$ [24]).

Note that, as shown in [24], by construction $\det(\mathbf{Z}^T\mathbf{b}_{\boldsymbol{\tau}_B})=0$, thus $\mathbf{Z}^T\mathbf{b}_{\boldsymbol{\tau}(s)}\to 0$ when $s\to s_f=1$, but this is a not a condition of existence of a conjugate point.

D. Application of the results to planar CDPRs

Planar CDPRs are usually considered as a degenerated case of the spatial general CDPRs. Accordingly, all previous mathematical derivations still apply, with several simplifications of the mathematical expressions, and even slight changes in the hypotheses that can be taken into account.

First, taking into account that the hypothesis of planar motions is totally true, i.e. that the full robot (including platform and cables) is entirely constrained to move into a plane, then the platform displacement group degenerates to $SE(2)$ which can be entirely parameterized by a vectorial space without any issue of representation singularities. This

simplifies the computation of the variations in Sections IV-B and IV-C.

Additionally, in the planar case, constant moments around the normal of the plane are conservative. Therefore, we may add a potential energy function related to these constant moments that must be taken into account when derivating the geometrico-, kinemato-static, and stability equations. For reasons of brevity, those equations are not provided in this paper, but they are given in the technical report [33].

It must be however mentioned that the hypothesis of planar motions is an *extremely* strong hypothesis, hard to achieve in reality. Indeed, it could be very difficult, and even impossible in reality, to impose that, even under small out-of-the-plane perturbations, the cables strictly stays into the plane of motion. If this hypothesis cannot be totally true, i.e. if cables can have out-of-the-plane motions under small perturbations, the planar motion hypothesis cannot be considered anymore for stability analysis purpose, and the equations given in Sections IV-B and IV-C must be used instead of those given in the technical report [33].

In the next section, we identify the link between stability and some of the singularities of CDPRs.

V. Stability and singularity

For identifying the robot singularities, let us first establish the equations of the kinemato-static model of the CDPR. In what follows, we show them for the general case of the spatial CDPR, but they can obviously be reduced to the planar case.

A. Kinemato-static model of the CDPR

In order to compute the kinemato-static model of the robot, let us take the variation of the vector $\mathbf{b}$ in (61) with respect to the unknowns of the geometrico-statics, that are: $\boldsymbol{g}_p$, $\boldsymbol{\tau}_B$ and $\boldsymbol{\ell} = [\ell_1 \dots \ell_n]^T$ ($\mathbf{x}_0$ being a fixed vector by mechanical design, its variation is null). We then get

$$\delta\mathbf{b} = \mathbf{0} = \begin{bmatrix} \text{tr}\left(b_1^T{}_{\boldsymbol{g}_p}\delta\boldsymbol{g}_p\right) \\ \vdots \\ \text{tr}\left(b_{3n+6}^T{}_{\boldsymbol{g}_p}\delta\boldsymbol{g}_p\right) \end{bmatrix} + \mathbf{b}_{\boldsymbol{\ell}}\delta\boldsymbol{\ell} + \mathbf{b}_{\boldsymbol{\tau}_B}\delta\boldsymbol{\tau}_B \tag{94}$$

where $\mathbf{b}_{\boldsymbol{\tau}_B} \in \mathbb{R}^{(3n+6)\times 3n}$ and $\mathbf{b}_{\boldsymbol{\ell}} \in \mathbb{R}^{(3n+6)\times n}$, the expression of $\mathbf{b}_\ell$ could be obtained by applying the methodology given in Section IV-C. Moreover, by using the results of the Eqs. (78) to (81), Eq. (94) can be modified as:

$$\mathbf{0} = \mathbf{J}_p\delta\boldsymbol{\Sigma}_p + \mathbf{b}_{\boldsymbol{\ell}}\delta\boldsymbol{\ell} + \mathbf{b}_{\boldsymbol{\tau}_B}\delta\boldsymbol{\tau}_B \tag{95}$$

Equation (95) is the *implicit kinemato-static model* which relates a variation of the platform configuration $\delta\boldsymbol{\Sigma}_p$ to a variation of the cable lengths $\delta\boldsymbol{\ell}$ and a variation of the cable tensions $\delta\boldsymbol{\tau}_B$.

We also have:

$$\mathbf{b}_{\boldsymbol{\tau}_B} = \frac{\partial\mathbf{b}}{\partial\boldsymbol{\tau}_B} = \frac{\partial\mathbf{b}}{\partial\boldsymbol{\tau}_0}\frac{\partial\boldsymbol{\tau}_0}{\partial\boldsymbol{\tau}_B} + \frac{\partial\mathbf{b}}{\partial\mathbf{x}_0}\frac{\partial\mathbf{x}_0}{\partial\boldsymbol{\tau}_B} \tag{96}$$

where $\boldsymbol{\tau}_0 = \boldsymbol{\tau}(s=0)$. It can be easily checked that $\partial\mathbf{x}_0/\partial\boldsymbol{\tau}_B = \mathbf{0}$. Moreover, as shown in Section IV-C, we also have $\partial\boldsymbol{\tau}_0/\partial\boldsymbol{\tau}_B = \mathbf{1}_{3n}$. Therefore,

$$\mathbf{b}_{\boldsymbol{\tau}_B} = \frac{\partial\mathbf{b}}{\partial\boldsymbol{\tau}_B} = \frac{\partial\mathbf{b}}{\partial\boldsymbol{\tau}_0} = \mathbf{b}_{\boldsymbol{\tau}_0} \tag{97}$$

As a result, Eq. (95) becomes

$$\mathbf{0} = \mathbf{J}_p\delta\boldsymbol{\Sigma}_p + \mathbf{b}_{\boldsymbol{\ell}}\delta\boldsymbol{\ell} + \mathbf{b}_{\boldsymbol{\tau}_0}\delta\boldsymbol{\tau}_B \tag{98}$$

which is the well-known implicit kinemato-static model of the robot [25].

From this equation, the *direct kinemato-static model* of the CDPR can be established:

$$\begin{bmatrix}\delta\boldsymbol{\Sigma}_p \\ \delta\boldsymbol{\tau}_B\end{bmatrix} = -\begin{bmatrix}\mathbf{J}_p & \mathbf{b}_{\boldsymbol{\tau}_0}\end{bmatrix}^{-1}\mathbf{b}_{\boldsymbol{\ell}}\delta\boldsymbol{\ell} \tag{99}$$

This expression is true as long as $\begin{bmatrix}\mathbf{J}_p & \mathbf{b}_{\boldsymbol{\tau}_0}\end{bmatrix} \in \mathbb{R}^{(3n+6)\times(3n+6)}$ is regular, as long as no singularity of the direct model appear. In what follows, we show that the singularities of the matrix $\begin{bmatrix}\mathbf{J}_p & \mathbf{b}_{\boldsymbol{\tau}_0}\end{bmatrix}$, which is up to a non singular matrix the Jacobian matrix of the direct kinemato-static equations, can be related to limits of stability.

It should be noted that, in case there is the same number of cables as degrees of freedom for the platform, the *inverse kinemato-static model* of the CDPR takes the form:

$$\begin{bmatrix}\delta\boldsymbol{\ell} \\ \delta\boldsymbol{\tau}_B\end{bmatrix} = -\begin{bmatrix}\mathbf{b}_{\boldsymbol{\ell}} & \mathbf{b}_{\boldsymbol{\tau}_0}\end{bmatrix}^{-1}\mathbf{J}_p\,\delta\boldsymbol{\Sigma}_p \tag{100}$$

where $\begin{bmatrix}\mathbf{b}_{\boldsymbol{\ell}} & \mathbf{b}_{\boldsymbol{\tau}_0}\end{bmatrix} \in \mathbb{R}^{(3n+6)\times(3n+6)}$ is regular, as long as there is no singularities of the inverse model.

B. Link between stability and singularities of the matrix $\begin{bmatrix}\mathbf{J}_p & \mathbf{b}_{\boldsymbol{\tau}_0}\end{bmatrix}$

When the matrix $\begin{bmatrix}\mathbf{J}_p & \mathbf{b}_{\boldsymbol{\tau}_0}\end{bmatrix}$ is singular, there exist small non null motions $\delta\boldsymbol{\Sigma}_p$ that belong to its kernel, for which $\delta\boldsymbol{\ell}$ is equal to 0.

These singularities correspond to robot configurations for which the end-effector cannot anymore resist to wrenches applied along given directions. These singularities can be related to the criterion of stability presented in Section (IV-C), as we will show here.

Let us consider the matrix $\mathbf{D} = \begin{bmatrix}\mathbf{Z}^T \\ \mathbf{J}_p^T\end{bmatrix} \in \mathbb{R}^{(3n+6)\times(3n+6)}$ where $\mathbf{Z}$ was defined in Eq. (90) as a matrix spanning the kernel of $\mathbf{J}_p^T$. As a result, the matrix $\mathbf{D}$ is square and always regular. We can thus left-multiply Eq. (98) by $\mathbf{D}$, leading to:

$$-\begin{bmatrix}\mathbf{Z}^T \\ \mathbf{J}_p^T\end{bmatrix}\mathbf{b}_{\boldsymbol{\ell}}\delta\boldsymbol{\ell} = \begin{bmatrix}\mathbf{Z}^T \\ \mathbf{J}_p^T\end{bmatrix}\begin{bmatrix}\mathbf{J}_p & \mathbf{b}_{\boldsymbol{\tau}_0}\end{bmatrix}\begin{bmatrix}\delta\boldsymbol{\Sigma}_p \\ \delta\boldsymbol{\tau}_B\end{bmatrix} \tag{101}$$

or also, by expanding this expression

$$-\begin{bmatrix}\mathbf{Z}^T \\ \mathbf{J}_p^T\end{bmatrix}\mathbf{b}_{\boldsymbol{\ell}}\delta\boldsymbol{\ell} = \begin{bmatrix}\mathbf{Z}^T\mathbf{J}_p & \mathbf{Z}^T\mathbf{b}_{\boldsymbol{\tau}_0} \\ \mathbf{J}_p^T\mathbf{J}_p & \mathbf{J}_p^T\mathbf{b}_{\boldsymbol{\tau}_0}\end{bmatrix}\begin{bmatrix}\delta\boldsymbol{\Sigma}_p \\ \delta\boldsymbol{\tau}_B\end{bmatrix} \tag{102}$$

$$= \begin{bmatrix}\mathbf{0}_{2n\times 3} & \mathbf{Z}^T\mathbf{b}_{\boldsymbol{\tau}_0} \\ \mathbf{J}_p^T\mathbf{J}_p & \mathbf{J}_p^T\mathbf{b}_{\boldsymbol{\tau}_0}\end{bmatrix}\begin{bmatrix}\delta\boldsymbol{\Sigma}_p \\ \delta\boldsymbol{\tau}_B\end{bmatrix} \tag{103}$$

$$= \mathbf{V}\begin{bmatrix}\delta\boldsymbol{\Sigma}_p \\ \delta\boldsymbol{\tau}_B\end{bmatrix} \tag{104}$$

with $\mathbf{Z}^T\mathbf{b}_{\boldsymbol{\tau}_0} = \mathbf{Z}^T\mathbf{b}_{\boldsymbol{\tau}}(s=0) \in \mathbb{R}^{3n\times 3n}$, $\mathbf{J}_p^T\mathbf{J}_p \in \mathbb{R}^{6\times 6}$, and $\mathbf{J}_p^T\mathbf{b}_{\boldsymbol{\tau}_0} \in \mathbb{R}^{6\times 3n}$. The matrix $\mathbf{V}$ being block-triangular with $\mathbf{Z}^T\mathbf{b}_{\boldsymbol{\tau}_0}$ and $\mathbf{J}_p^T\mathbf{J}_p$ square, its determinant is equal to:

$$\det(\mathbf{V}) = \det(\mathbf{Z}^T\mathbf{b}_{\boldsymbol{\tau}_0})\det(\mathbf{J}_p^T\mathbf{J}_p) \tag{105}$$

Moreover, the matrix $\mathbf{Z}$ being regular by construction, the matrix $\mathbf{V}$ has the same singularities as the matrix $\begin{bmatrix}\mathbf{J}_p & \mathbf{b}_{\boldsymbol{\tau}_0}\end{bmatrix}$. As a result, the singularities of the matrix $\begin{bmatrix}\mathbf{J}_p & \mathbf{b}_{\boldsymbol{\tau}_0}\end{bmatrix}$ can appear if and only if at least one of the two following conditions appear:

- The matrix $\mathbf{J}_p$ is singular: It can be proven by using algebraic tools [34] that this matrix is singular if and only if all passive spherical joints in points B_i are aligned (in the spatial case) or superposed (in the planar case). In this case, the robot is architecturally singular as the rotation of the platform around this line cannot be controlled.
- The matrix $\mathbf{Z}^T\mathbf{b}_{\boldsymbol{\tau}_0}$ is singular: From Section IV-C, this conditions means the appearance of a conjugate point at $s = 0$. A conjugate point at $s = 0$ is a limit case of stability, as discussed in [24]: if no conjugate point appears for $s \in [0\ 1[$, the robot is stable, and if there is a conjugate point on this interval, the robot is unstable. If in a singularity of $\begin{bmatrix}\mathbf{J}_p & \mathbf{b}_{\boldsymbol{\tau}_0}\end{bmatrix}$, a conjugate point appears at $s = 0$, this means that these singularities separate the sets of stable and unstable configurations.

We highlight the theoretical results in the next section.

VI. Case Study

In this section, we analyze the stability of a spatial six-cable CDPR (Fig. 3). This robot is made of six cables, each being connected to the ground at points A_i. The cable extremities are linked to a rigid moving platform by a second passive spherical joint (points B_i). This suspended robot having six motors, we may control the position and orientation of the platform frame $\mathcal{F}_p$. In what follows, in order to have a more intuitive reporting of the platform orientation, the orientation is provided by the Roll, Pitch and Yaw angles (i.e. a 3-2-1 Euler angle rotation sequence) denoted as φ_p, θ_p and ψ_p respectively, but all computations are still rigorously made based on the Lie group differentiation shown in the previous section when providing the numerical results.

For the studied robot, positions of points A_i in the base frame $\mathcal{F}_0$ are given by: $\overrightarrow{OA_i} = r_b\,[\cos\gamma_i\ \sin\gamma_i\ 0]^T$ $(i = 1,2,3)$ with $r_b = 1$ m and $\gamma_1 = 0$, $\gamma_2 = 2\pi/3$, and $\gamma_3 = -2\pi/3$. Positions of points B_i are given in the platform frame $\mathcal{F}_p$ by:

$$\overrightarrow{PB_1} = [0.2\ 0\ 0]^T,\ \overrightarrow{PB_2} = [-0.2\ 0.2\ 0]^T,\ \overrightarrow{PB_3} = [-0.2\ 0\ 0]^T$$
$$\overrightarrow{PB_4} = [0.2\ 0\ 0]^T,\ \overrightarrow{PB_5} = [0\ 0\ 0.2]^T,\ \overrightarrow{PB_6} = [0\ 0.2\ 0.2]^T$$

All point coordinates are in meters. The cable properties are: Young's modulus $E = 100$ GPa, cable cross-section radius $r = 2$ mm, material density $\rho/A = 1571$ kg/m^3. The platform mass is equal to $m_p = 0.5$ kg. There is no external force except gravity applied on the platform.

In order to analyze the stability of this robot, we first compute the end-effector configuration space at a given altitude $z_p = -0.746$ m and orientation $\varphi_p = -1.531$ rad, $\theta_p = 0.870$ rad, $\psi_p = 0.443$ rad. For this, we compute sets of configurations $(\boldsymbol{\ell}, \boldsymbol{g}_p, \boldsymbol{\tau}_B)$ connected to an initial configuration $(\boldsymbol{\ell}_{\text{init}}, \boldsymbol{g}_{p\ \text{init}}, \boldsymbol{\tau}_{B\ \text{init}})$, by using a continuation algorithm [35].

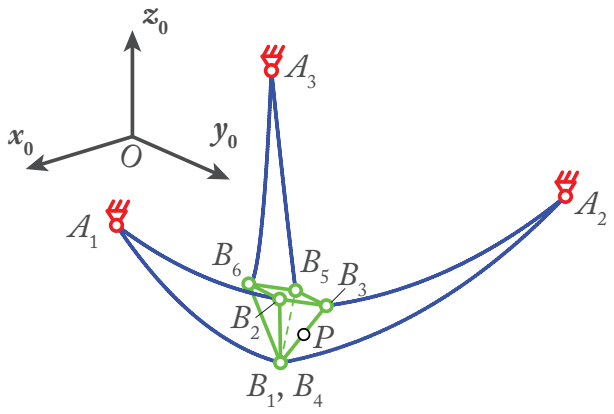

Fig. 3. Schematics of the spatial six-cable CDPR under study (to scale).

For every configurations of the computed configuration space, the inverse condition numbers κ_ℓ^{-1} and κ_p^{-1} of matrices $\begin{bmatrix}\mathbf{b}_{\boldsymbol{\ell}} & \mathbf{b}_{\boldsymbol{\tau}_0}\end{bmatrix}$ and $\begin{bmatrix}\mathbf{J}_p & \mathbf{b}_{\boldsymbol{\tau}_0}\end{bmatrix}$, respectively, are calculated. For a better display by color in Fig. 4, instead of showing directly κ_ℓ^{-1} and κ_p^{-1}, we provide their value at a given power: κ_ℓ^{-2} and $\kappa_p^{-0.6}$. Dark blue zones are zones with bad inverse condition numbers. The results show that:

- The matrix $\begin{bmatrix}\mathbf{b}_{\boldsymbol{\ell}} & \mathbf{b}_{\boldsymbol{\tau}_0}\end{bmatrix}$ loses its rank, i.e. the inverse condition number κ_ℓ^{-1} drops down to zero, near the end-effector configuration space boundaries.
- The matrix $\begin{bmatrix}\mathbf{J}_p & \mathbf{b}_{\boldsymbol{\tau}_0}\end{bmatrix}$ loses its rank, i.e. the inverse condition number κ_p^{-1} drops down to zero, inside the end-effector configuration space (Fig. 4(b)). Singularities of $\begin{bmatrix}\mathbf{J}_p & \mathbf{b}_{\boldsymbol{\tau}_0}\end{bmatrix}$ are suspected here.

In Figure 5, we show the robot end-effector configuration space, for the platform altitude $z_p = -0.746$ m and orientation $\varphi_p = -1.531$ rad, $\theta_p = 0.870$ rad, $\psi_p = 0.443$ rad. In this picture, in particular, we highlight in red the area where the inverse condition number of $\begin{bmatrix}\mathbf{J}_p & \mathbf{b}_{\boldsymbol{\tau}_0}\end{bmatrix}$ is lower than $15 \cdot 10^{-4}$, i.e. near which singularities of $\begin{bmatrix}\mathbf{J}_p & \mathbf{b}_{\boldsymbol{\tau}_0}\end{bmatrix}$ are foreseen to be present. This red zone separates the end-effector configuration space into two connected components. For assessing the presence of singularities in the red zones, we define a path between points $Q_1 = (-0.33,\ -0.18)$ m and $Q_3 = (-0.35,\ -0.20)$ m (Fig. 5) along which the stability criterion defined previously will be computed. Along this path, 100 points are defined. From Figs. 6(a) to 6(f), we observe the following things:

- In point Q_1, the sign of the determinant of the matrix $\mathbf{Z}^T\mathbf{b}_{\boldsymbol{\tau}(s)}$ is always positive on the interval $[0\,1[$: there is no conjugate point associated with this configuration, which is stable.
- In point Q_3, the sign of the determinant of the matrix $\mathbf{Z}^T\mathbf{b}_{\boldsymbol{\tau}(s)}$ varies. It is negative on the interval $[0\,0.125]$ and positive on $[0.125\,1[$: there is a conjugate point associated with this configuration, which is then unstable.

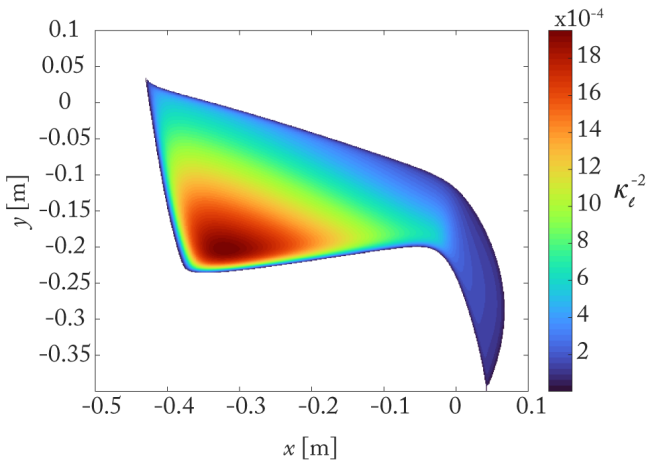

(a) Inverse condition number of $\begin{bmatrix}\mathbf{b}_{\boldsymbol{\ell}} & \mathbf{b}_{\boldsymbol{\tau}_0}\end{bmatrix}$ at the power 2

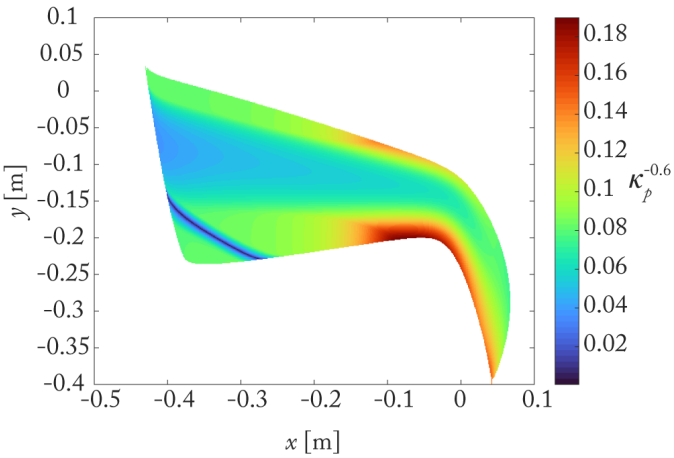

(b) Inverse condition number of $\begin{bmatrix}\mathbf{J}_p & \mathbf{b}_{\boldsymbol{\tau}_0}\end{bmatrix}$ at the power 0.6

Fig. 4. Inverse condition numbers for the matrices $\begin{bmatrix}\mathbf{b}_{\boldsymbol{\ell}} & \mathbf{b}_{\boldsymbol{\tau}_0}\end{bmatrix}$ and $\begin{bmatrix}\mathbf{J}_p & \mathbf{b}_{\boldsymbol{\tau}_0}\end{bmatrix}$ for the spatial six-cable CDPR in its end-effector configuration space, for a platform altitude $z_p = -0.746$ m and orientation $\varphi_p = -1.531$ rad, $\theta_p = 0.870$ rad, $\psi_p = 0.443$ rad.

- There is a point Q_2 where a conjugate point appears on the integration interval at $s = 0$, meaning that there is a singularity of the matrix $\begin{bmatrix}\mathbf{J}_p & \mathbf{b}_{\boldsymbol{\tau}_0}\end{bmatrix}$.

The red area computed using the continuation algorithm provides only an indication of the presence of singularity curve for $\begin{bmatrix}\mathbf{J}_p & \mathbf{b}_{\boldsymbol{\tau}_0}\end{bmatrix}$. However, the change in the number of conjugate points actually proves the presence of this curve. Furthermore a simple dichotomy process could allow to determine two poses Q_{2a}, Q_{2b} with a distance between these poses lower than an arbitrary threshold and such that it is guaranteed to have a congugate point between them. Moreover, the existence of these singularity curves and the presence of no or a conjugate point allow also to conclude that:

- Zone $\mathcal{A}$ is the zone of the stable configurations,
- Zone $\mathcal{B}$ is the zone of the unstable configurations.

Because there is no possibility to check the stability of the solutions of the Irvine's model itself except applying the theory presented in this paper, in order to definitely validate

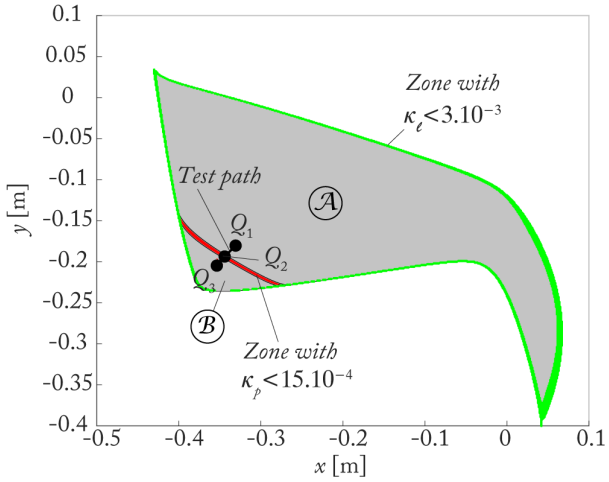

Fig. 5. Stable and unstable end-effector configuration spaces of the spatial six-cable CDPR, for a platform altitude $z_p = -0.646$ m and orientation $\varphi_p = -2.578$ rad, $\theta_p = 0.608$ rad, $\psi_p = 0.442$ rad. In green, the areas where the inverse condition number of $\begin{bmatrix}\mathbf{b}_{\boldsymbol{\ell}} & \mathbf{b}_{\boldsymbol{\tau}_0}\end{bmatrix}$ is lower than $3 \cdot 10^{-3}$; in red, the areas where the inverse condition number of $\begin{bmatrix}\mathbf{J}_p & \mathbf{b}_{\boldsymbol{\tau}_0}\end{bmatrix}$ is lower than $15 \cdot 10^{-4}$.

TABLE I
MAXIMAL ERROR OF MODELLING FOR THE LUMPED CABLE MODEL WITH RESPECT TO THE IRVINE'S MODEL, AS A FUNCTION OF THE NUMBER N OF ELEMENTS USED PER CABLE.

	$N=2$	$N=5$	$N=10$	$N=15$	$N=30$	$N=60$
Err. [mm]	54.65	7.31	1.83	0.81	0.20	0.05

these results on the stability prediction, we developed a *static* lumped model of our robot [36]. Each cable is now discretized with N elements. The robot potential energy becomes then an analytic function of the finite element variables plus the platform configuration variables, instead of a functional. As a result, checking the stability of the lumped model configuration remains to checking the positive-definiteness of the reduced Hessian of the energy, as it has been done in [37] for assessing the stability of continuum parallel robots, or in [20] for checking the stability of the straight-cable underactuated CDPRs.

First, in order to assert the lumped model validity, we check its configuration prediction accuracy. For doing this, we compute the length of the cables based of the Irvine's model for each of the 100 configurations along the chosen path between points Q_1 and Q_3. Then, we reperform the same computation, but with the lumped model. Results for the maximal cable length estimation error are summuarized in Tab. I for several values of numbers of elements used per cables in the lumped model. With 60 elements per cable, this error is lower than $1 \cdot 10^{-4}$ m for all cables (which all measure several meters). This error of prediction between the two models is negligible, and 60 elements per cables are used for the remaining of this work.

Then, we compute the smallest eigenvalue σ_1 of the reduced Hessian of the lumped model's potential energy and we check its positiveness all along the path between configurations Q_1 and Q_3 (Fig. 7). We compare this value at each robot

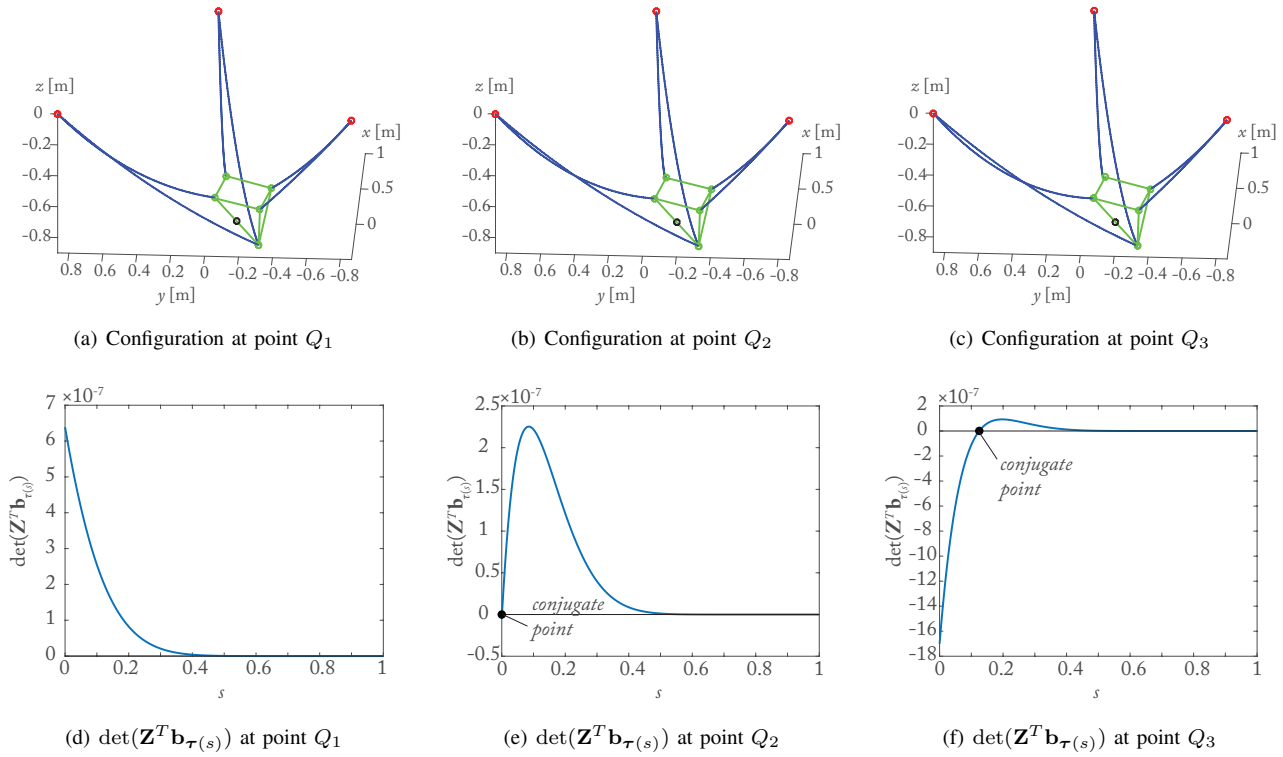

(a) Configuration at point Q_1 (b) Configuration at point Q_2 (c) Configuration at point Q_3

(d) $\det(\mathbf{Z}^T\mathbf{b}_{\boldsymbol{\tau}(s)})$ at point Q_1 (e) $\det(\mathbf{Z}^T\mathbf{b}_{\boldsymbol{\tau}(s)})$ at point Q_2 (f) $\det(\mathbf{Z}^T\mathbf{b}_{\boldsymbol{\tau}(s)})$ at point Q_3

Fig. 6. Study of the determinant of the matrix $\mathbf{Z}^T\mathbf{b}_{\boldsymbol{\tau}(s)}$ all along the path between points Q_1 and Q_3.

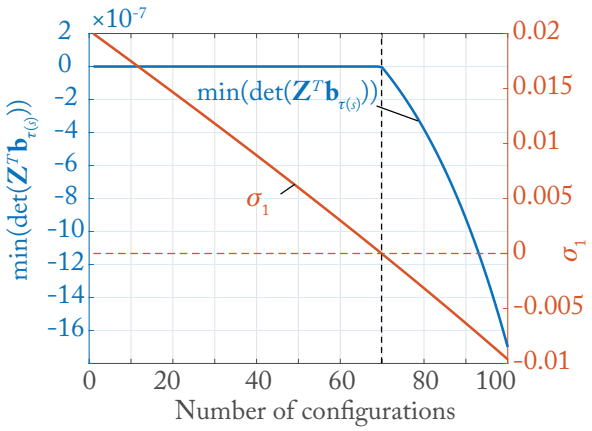

Fig. 7. Comparison at each configuration all along the path of the stability prediction based on the Jacobi condition computed on the Irvine's model (computation of $\min(\det(\mathbf{Z}^T\mathbf{b}_{\boldsymbol{\tau}(s)}))$ on the integration interval $s \in [0\ 1[$) with a stability prediction based on a lumped model (computation of the smallest eigenvalue σ_1 of the Hessian of the potential energy).

configuration with the minimal value of $\det(\mathbf{Z}^T\mathbf{b}_{\boldsymbol{\tau}(s)})$ on the interval $s \in [0,\ 1[$. We see that, up to the configuration 70 (point Q_2), the smallest eigenvalue σ_1 is positive, indicating the configurations are stable, which is confirmed by the fact there is no conjugate points for the Irvine's model (Fig. 6(d)). In point Q_2, σ_1 is null, which corresponds to the appearance of the conjugate point at $s = 0$ (Fig. 6(e)). Between Q_2 and Q_3, σ_1 is negative, showing that the robot modelled with the lumped cables is unstable, as it was also detected thanks to the Jacobi criterion on the Irvine's model (Fig. 6(f)).

We also checked that there are multiple solutions to the inverse geometrico-static model at the extremities of the trajectories Q_1 and Q_3 by using interval analysis [19]. Two other solutions were found for each platform configurations. Two of them are stable (denoted as Q_{13} and Q_{33}), the two other are unstable (denoted as Q_{12} and Q_{32}): some conjugate points exist when analyzing these last two configurations (Fig. 8). In the stable solutions Q_{13} and Q_{33}, some cable lengths are much higher than in the previous solution. We tried to move from the three solutions associated with the platform configurations Q_3 to the three solutions associated with the platform configurations Q_1 by using the direct geometrico-static model: from Q_{32} we came back to Q_{12}, from Q_{33} to Q_{13} while the other (initial) solutions to Q_1 and Q_3 seem disconnected from the other configurations. As a result, this tends to say that the unstable (stable, resp.) solutions Q_{32} and Q_{12} (Q_{33} and Q_{13}, resp.) belongs to the same aspect. However, further investigations on this issue are necessary, but left as a future work. All these results show the validity of our approach.

Finally, we wanted to check if the singularities of the kinemato-static models of the sagging CDPRs had something in common with the traditional singularities of rigid-link parallel robots appearing when the system of wrenches applied on the platform was degenerated [38]. For this, we computed the inverse condition number κ_W^{-1} of the wrench matrix $\mathbf{W}$

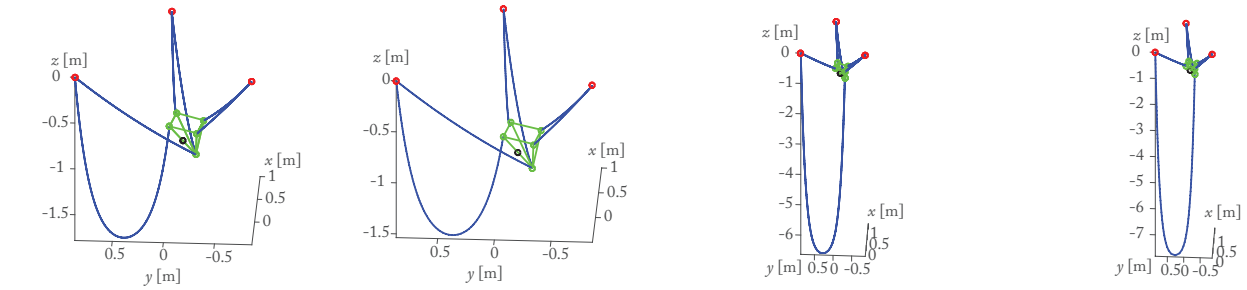

(a) Second solution Q_{12} of the inverse geometrico-static model at Q_1 (unstable)

(b) Second solution Q_{32} of the inverse geometrico-static model at Q_3 (unstable)

(c) Third solution Q_{13} of the inverse geometrico-static model at Q_1 (stable)

(d) Third solution Q_{33} of the inverse geometrico-static model at Q_3 (stable)

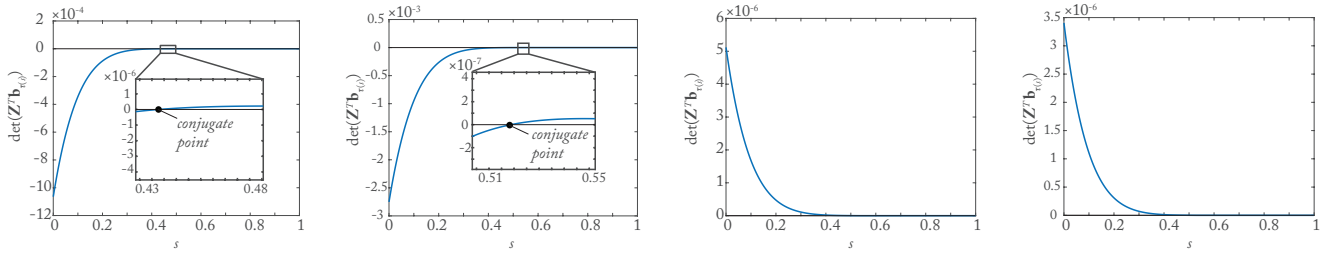

(e) $\det(\mathbf{Z}^T\mathbf{b}_{\boldsymbol{\tau}(s)})$ at point Q_{12}

(f) $\det(\mathbf{Z}^T\mathbf{b}_{\boldsymbol{\tau}(s)})$ at point Q_{32}

(g) $\det(\mathbf{Z}^T\mathbf{b}_{\boldsymbol{\tau}(s)})$ at point Q_{13}

(h) $\det(\mathbf{Z}^T\mathbf{b}_{\boldsymbol{\tau}(s)})$ at point Q_{33}

Fig. 8. Other solutions of the inverse geometrico-static model at Q_1 and Q_3 and verification of their stability property.

defined as:

$$\mathbf{W} = \begin{bmatrix} \boldsymbol{\tau}_{B_1}^T & ([^0\overrightarrow{PB_1}]^\wedge \boldsymbol{\tau}_{B_1})^T \\ \vdots & \vdots \\ \boldsymbol{\tau}_{B_6}^T & ([^0\overrightarrow{PB_6}]^\wedge \boldsymbol{\tau}_{B_6})^T \end{bmatrix} \tag{106}$$

We compared its inverse condition number with the ones of the matrices $\begin{bmatrix}\mathbf{b}_{\boldsymbol{\ell}} & \mathbf{b}_{\boldsymbol{\tau}_0}\end{bmatrix}$ and $\begin{bmatrix}\mathbf{J}_p & \mathbf{b}_{\boldsymbol{\tau}_0}\end{bmatrix}$ all along the path between Q_1 and Q_3 (first solution). The results are provided in Fig. 9 and they show that there is no coincidence between the loss of rank of $\mathbf{W}$ and the losses of rank of the matrices $\begin{bmatrix}\mathbf{b}_{\boldsymbol{\ell}} & \mathbf{b}_{\boldsymbol{\tau}_0}\end{bmatrix}$ and $\begin{bmatrix}\mathbf{J}_p & \mathbf{b}_{\boldsymbol{\tau}_0}\end{bmatrix}$. The inverse condition number of $\begin{bmatrix}\mathbf{J}_p & \mathbf{b}_{\boldsymbol{\tau}_0}\end{bmatrix}$ vanishes at the configuration 70, while for $\begin{bmatrix}\mathbf{b}_{\boldsymbol{\ell}} & \mathbf{b}_{\boldsymbol{\tau}_0}\end{bmatrix}$ it never crosses zero, as expected. For $\mathbf{W}$, inverse condition number is never null. This means that **the singularities of the wrench system are not singularities of the forward kinemato-static model of the sagging CDPRs, contrary to what happens in rigid-link parallel robotics.**

Note that the Matlab code for computing the stability of the robot configuration is provided as an external material, as well as a Maple code for localizing the neighbourhood of singular configurations.

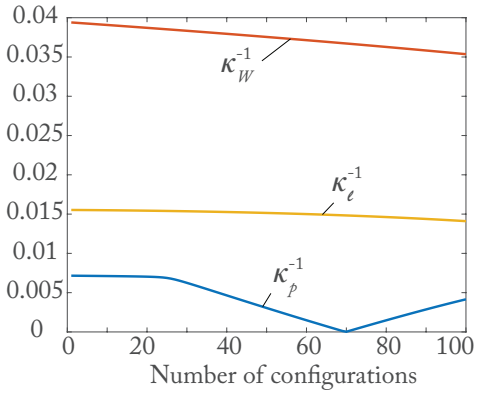

Fig. 9. Inverse condition numbers κ_W^{-1}, κ_ℓ^{-1} and κ_p^{-1} of the matrices $\mathbf{W}$, $\begin{bmatrix}\mathbf{b}_{\boldsymbol{\ell}} & \mathbf{b}_{\boldsymbol{\tau}_0}\end{bmatrix}$ and $\begin{bmatrix}\mathbf{J}_p & \mathbf{b}_{\boldsymbol{\tau}_0}\end{bmatrix}$, respectively, all along the path between points Q_1 and Q_3.

VII. Conclusion

This paper dealt with the stability analysis of sagging CDPRs and with its links to robot singularities, using the Irvine's cable model. As any underactuated mechanical system at a given pose the system may be stable or unstable and, with the Irvine's cable model which is the solution to an ODE, assessing the stability of a configuration cannot be done by checking the eigenvalues of a stiffness matrix associated with the platform displacement under the application of external loadings.

In the present paper, to the best of our knowledge, we have shown for the first time that the geometrico-static equations of the sagging CDPRs are local extrema of the functional describing the robot potential energy. For assessing the stability of the robot configuration, it was then necessary to check two types of conditions: The Legendre-Clebsch conditions coupled with the Jacobi conditions, which are well known in optimal control theory. We shown that, in normal conditions on Earth (except under water), the Legendre-Clebsch conditions are always verified. Moreover, we proved that singularities of the forward geometrico-static model of the CDPRs are limits of stability.

In order to validate the theoretical results, we compared the stability prediction based on the Jacobi criterion with results coming from a lumped model of the CDPRs. For this discretized model, the stability can be checked by verifying the positive-definiteness of a reduced Hessian matrix of the potential energy. We first checked the accuracy of the lumped model with respect to the results provided by the Irvine's model, and we then verified that the smallest eigenvalues of the reduced Hessian changed their signs when conjugate points appeared (Jacobi criterion). We also found that singularities of the platform wrench system are not singularities of the forward kinemato-static models of the sagging CDPRs, contrary to what happens in rigid-link parallel robotics.

Further work will deal with the analysis of the dynamics of sagging CDPRs, and the better analysis of the phenomena appearing when singularities of the inverse geometrico-static model exist. We will also devote some efforts on the analysis of the connectivity between the workspace aspects, especially those containing only stable configurations. This would pave the way to a better calculation of CDPRs workspace which is crucial for the design phase. Instead of relying only on the inverse model with its multiple solutions we may check the connectivity between the workspace aspects having only stable configurations to establish the reachable workspace.

APPENDIX

A. Recalls on Lie group notations

Some notational conventions of Lie group theory are recalled here for reasons of convenience. A hat "$\wedge$" covering a vector $\boldsymbol{\Upsilon}$ defines a matrix $\hat{\boldsymbol{\Upsilon}}$ whose expression depends on the dimension of $\boldsymbol{\Upsilon}$. If $\boldsymbol{\Upsilon} \in \mathbb{R}^3$, then $\hat{\boldsymbol{\Upsilon}} = \boldsymbol{\Upsilon}^\wedge$ denotes the (3×3) skew symmetric matrix defined such that: $\hat{\boldsymbol{\Upsilon}}\mathbf{x} = \boldsymbol{\Upsilon}\times\mathbf{x}$ for any $\mathbf{x} \in \mathbb{R}^3$. If $\boldsymbol{\Upsilon} = [\mathbf{a}^T\ \mathbf{b}^T]^T \in \mathbb{R}^6$, with $\mathbf{a},\ \mathbf{b} \in \mathbb{R}^3$, then $\hat{\boldsymbol{\Upsilon}}$ is the (4×4) matrix defined by:

$$\hat{\boldsymbol{\Upsilon}} = \begin{bmatrix} \hat{\mathbf{b}} & \mathbf{a} \\ \mathbf{0}_{1\times3} & 0 \end{bmatrix} \tag{107}$$

Reciprocally, the superscript "$\vee$" is such that $\hat{\boldsymbol{\Upsilon}}^\vee = \boldsymbol{\Upsilon}$ for any $\boldsymbol{\Upsilon} \in \mathbb{R}^3$ or $\mathbb{R}^6$.

Let us consider that a group $\boldsymbol{g}$ is a function of a variable t, i.e. $\boldsymbol{g} = \boldsymbol{g}(t)$. Then, we may define the vector $\mathbf{t}$ by any of the following relations

$$\mathbf{t} = \left(\boldsymbol{g}^{-1}\frac{\partial \boldsymbol{g}}{\partial t}\right)^\vee \tag{108}$$

or also

$$\boldsymbol{g}\,\hat{\mathbf{t}} = \frac{\partial \boldsymbol{g}}{\partial t} \tag{109}$$

Let us assume that $\boldsymbol{g} \in SE(3)$. In this case, $\mathbf{t} \in se(3) \cong \mathbb{R}^6$ is a vector made of two parts such that $\mathbf{t} = [\boldsymbol{\omega}^T\ \mathbf{v}^T]^T$, where $\boldsymbol{\omega} \in \mathbb{R}^3$ corresponds to the rate of change of orientation with respect to the variable t, while $\mathbf{v} \in \mathbb{R}^3$ corresponds to the rate of change of position with respect to the variable t. Obviously, if the variable t represents the time, $\mathbf{t}$ is a twist, $\boldsymbol{\omega}$ a rotational velocity, and $\mathbf{v}$ a translation velocity.

It should be mentioned that, by using the expressions (108) and (109), $\mathbf{t}$, $\boldsymbol{\omega}$ and $\mathbf{v}$ are expressed in a local frame.

REFERENCES

[1] S. Landsberger and T. Sheridan, "A minimal, minimal linkage: the tension-compression parallel link manipulator," in *IMACS/SICE Int. Symp. on Robotics, Mechatronics, and Manufacturing Systems*, Kobe, September, 16-20, 1992, pp. 493–500.

[2] J. Albus, R. Bostelman, and N. Dagalakis, "The NIST SPIDER, a robot crane," *Journal of research of the National Institute of Standards and Technology*, vol. 97, no. 3, pp. 373–385, May 1992.

[3] S. Kawamura *et al.*, "High-speed manipulation by using parallel wire-driven robots," *Robotica*, vol. 18, no. 1, pp. 13–21, January 2000.

[4] T. Bruckmann *et al.*, "Development of a storage retrieval machine for high racks using a wire robot," in *ASME DETC*, Chicago, 2012.

[5] A. Pott *et al.*, "Cable-driven parallel robots for industrial applications: the IPAnema system family," in *ISR*, 2013.

[6] M. Gouttefarde *et al.*, "Simplified static analysis of large-dimension parallel cable-driven robots," in *IEEE Int. Conf. on Robotics and Automation*, Saint Paul, May, 14-18, 2012, pp. 2299–2305.

[7] A. Martin, S. Caro, and P. Cardou, "Design of a cable-driven parallel robot with grasping device," in *28th CIRP Design Conf.*, Nantes, 2018.

[8] J.-P. Merlet, "MARIONET, a family of modular wire-driven parallel robots," in *ARK*, Piran, June 28- July 1, 2010, pp. 53–62. [Online]. Available: http://www-sop.inria.fr/coprin/PDF/ark2010.pdf

[9] S. Baklouti, S. Caro, and E. Courteille, "Dynamic and oscillatory motions of cable-driven parallel robots based on a non-linear cable tension model," *J. of Mechanisms and Robotics*, vol. 9, September 2017.

[10] J. Begey *et al.*, "Dynamic control of parallel robot driven by flexible cables and actuated by position-controlled winches," *IEEE Trans. on Robotics*, vol. 35, no. 1, pp. 286–293, February 2019.

[11] I. Chawla *et al.*, "Effect of selection criterion on the kineto-static solution of a redundant cable-driven parallel robot considering cable mass and elasticity," *Mechanism and Machine Theory*, vol. 156, 2021.

[12] V. Ferravante *et al.*, "Dynamic analysis of high precision construction cable-driven parallel robots," *Mechanism and Machine Theory*, vol. 135, pp. 54–64, 2019.

[13] P. Miermeister *et al.*, "An elastic cable model for cable-driven parallel robots including hysteresis effect," in *2nd Int. Conf. on cable-driven parallel robots (CableCon)*, Duisburg, August, 24-27, 2014, pp. 17–28.

[14] J. Piao *et al.*, "Open-loop position control of a polymer cable-driven parallel robot via a viscoelastic cable model for high payload workspaces," *Advances in Mechanical Engineering*, vol. 9, no. 12, 2017.

[15] H. M. Irvine, *Cable Structures*. MIT Press, 1981.

[16] N. Riehl *et al.*, "On the determination of cable characteristics for large dimension cable-driven parallel mechanisms," in *IEEE Int. Conf. on Robotics and Automation*, Anchorage, May, 3-8, 2010, pp. 4709–4714.

[17] J.-P. Merlet, "A new generic approach for the inverse kinematics of cable-driven parallel robot with 6 deformable cables," in *ARK*, Grasse, June, 27-30, 2016. [Online]. Available: http://www-sop.inria.fr/hephaistos/PDF/merlet_ark2016.pdf

[18] ——, "Preliminaries of a new approach for the direct kinematics of suspended cable-driven parallel robot with deformable cables," in *Eucomes*, Nantes, September, 20-23, 2016.

[19] ——, "On the inverse kinematics of cable-driven parallel robots with up to 6 sagging cables," in *IEEE Int. Conf. on Intelligent Robots and Systems (IROS)*, Hamburg, Germany, September 28- October 2, 2015, pp. 4536–4361.

[20] M. Carricato and J.-P. Merlet, "Stability analysis of underconstrained cable-driven parallel robots," *IEEE Trans. on Robotics*, vol. 29, no. 1, pp. 288–296, 2013. [Online]. Available: http://www-sop.inria.fr/coprin/PDF/tro_carricato_2013.pdf

[21] H. Wei, Y. Qiu, and J. Yang, "An approach to evaluatestability for cable-based parallelcamera robots with hybrid tension-stiffness properties," *International Journal of Advanced Robotic Systems*, vol. 12, no. 12, 2015.

[22] P. Liu and H. Ma, "On the stability for a cable-driven parallel robotwhile considering the cable sag effects," in *Proceedings of the 2016 13th International Conference on Ubiquitous Robots and Ambient Intelligence (URAl)*, Sofitel Xian on Renmin Square, Xian, China, Aug. 2016, pp. 538–543.

[23] J. Till and D. Rucker, "Elastic stability of Cosserat rods and parallel continuum robots," *IEEE Transactions on Robotics*, vol. 33, no. 3, pp. 718–733, 2017.
[24] D. Hull, *Optimal Control Theory for Applications*, F. Ling, Ed. New York, NY, USA: Oxford University Press: Springer, 2003.
[25] J.-P. Merlet, "Singularity of cable-driven parallel robot with sagging cables: preliminary investigation," in *Proceedings of the IEEE 2019 International Conference on Robotics and Automation (ICRA 2019)*, Montreal, Canada, May 2019, pp. 504–509.
[26] C. Quennouelle and C. Gosselin, "Kinematostatic modeling of compliant parallel mechanisms," *Meccanica*, vol. 46, no. 1, pp. 155–169, jan 2011.
[27] A. A. Shabana, *Dynamics of multibody systems*. Cambridge University Press, 2009.
[28] H. Ziegler, *Principles of Structural Stability*. Cambridge, MA, USA: Birkhäuser, 1977, ch. 1, p. 30.
[29] E. Gekeler, *Mathematical Methods for Mechanics: A Handbook with MATLAB Experiments*. Springer-Verlag Berlin Heidelberg: Springer, 2008.
[30] D. Holm, *Geometric Mechanics and Symmetry: From Finite to Infinite-Dimensions*. New York, NY, USA: Oxford Univ. Press, 2009.
[31] J.-P. Merlet and J. di Sandretto, "The forward kinematics of cable-driven parallel robots with sagging cables," in *Mechanisms and Machine Science*. Springer International Publishing, aug 2014, pp. 3–15.
[32] J.-P. Merlet, "On the inverse kinematics of cable-driven parallel robots with up to 6 sagging cables," in *2015 IEEE/RSJ International Conference on Intelligent Robots and Systems (IROS 2015)*. IEEE, sep 2015.
[33] S. Briot and J.-P. Merlet, "Direct kinematic singularities and stability analysis of planar sagging cable-driven parallel robots," Laboratoire des Sciences du Numérique de Nantes (LS2N), UMR CNRS 6004; Inria Sophia Antipolis, Tech. Rep., 2022. [Online]. Available: https://hal.science/hal-04007182
[34] D. Cox, J. Little, and D. OShea, *Ideals, varieties, and algorithms: an introduction to computational algebraic geometry and commutative algebra*. Springer Science & Business Media, 2013.
[35] K. G. Eugene L. Allgower, *Numerical Continuation Methods*. Springer Berlin Heidelberg, Oct. 2011. [Online]. Available: https://www.ebook.de/de/product/19302145/eugene_l_allgower_kurt_georg_numerical_continuation_methods.html
[36] T. K. Mamidi and S. Bandyopadhyay, "Forward dynamic analyses of cable-driven parallel robots with constant input with applications to their kinetostatic problems," *Mechanism and Machine Theory*, vol. 163, p. 104381, 2021.
[37] S. Briot and A. Goldsztejn, "Singularity conditions for continuum parallel robots," *IEEE Transactions on Robotics*, vol. 38, no. 1, pp. 507–525, 2022.
[38] J.-P. Merlet, "Singular configurations of parallel manipulators and Grassmann geometry," *The International Journal of Robotics Research*, vol. 8, no. 5, pp. 45–56, 1989.

Sébastien Briot received the B.S. and M.S. degrees in mechanical engineering in 2004 and the Ph.D. degree in robotics in 2007, from the Institut National des Sciences Appliquées de Rennes, Rennes, France. He was a Postdoctoral Fellow with the Ecole de Technologie Supérieure, Montreal, QC, Canada, in 2008. In 2009, he has been recruited at CNRS as a researcher in the Laboratoire des Sciences du Numérique de Nantes, Nantes, France, where he has been the Head of the ARMEN Research Team since 2017. Since 2022, he is CNRS Director of Research in the same lab. He has authored more than 50 referred journal papers, two books, and four inventions. His research interests include the design optimization of robots and the analysis of their performance, especially their singularities. Dr. Briot received the Best Ph.D. Thesis Award in Robotics from the French CNRS in 2007. In 2011, he received two other awards: the Award for the Best Young Researcher from the French Region Bretagne and the Award for the Best Young Researcher from the French Section of the American Society of Mechanical Engineering.

Jean-Pierre Merlet is a senior scientist at INRIA, the French National Research Institute in Computer Science and Control theory. He received his Engineer title from the Ecole Centrale de Nantes in 1980, his PhD in 1986 from Paris VI University and his Research habilitation from Nice University in 1993.

He has worked as an engineer in the food industry (Lu) and in civil engineering. He has worked as research engineer at the CEA (French nuclear Agency) and as research associate in Japan (Kyoto University, MEL, Tsukuba) and in Canada (McGill University, Montreal). He his now team leader of the HEPHAISTOS project of INRIA.

J-P. Merlet is the author of over 300 conference papers and over 60 journal papers in the field of force control of robots, algebraic geometry, mechanism history, constraints solving, robotics and art, AI and parallel robots. He has published a reference book on this later subject with 2 editions in French and two editions in English.

J-P. Merlet is an IEEE Fellow and received the IFToMM Award of Merits and is doctor honoris causae from Innsbruck University.